THE UNIVERSITY OF ALBERTA

THERMALLY LOADED CIRCULAR PLATES BY MOIRÉ METHOD

by

KANWAL RAJ SINGH JAWANDA, B.A. (Panjab), B.Sc. (Glasgow)

A THESIS

SUBMITTED TO THE FACULTY OF GRADUATE STUDIES

IN PARTIAL FULFILMENT OF THE REQUIREMENTS FOR THE DEGREE OF

MASTER OF SCIENCE

DEPARTMENT OF MECHANICAL ENGINEERING

EDMONTON, ALBERTA

DECEMBER, 1965

UNIVERSITY OF ALBERTA

FACULTY OF GRADUATE STUDIES

The undersigned certify that they have read, and recommend to the Faculty of Graduate Studies for acceptance, a thesis entitled, "THERMALLY LOADED CIRCULAR PLATES BY MOIRÉ METHOD" submitted by Kanwal Raj Singh Jawanda in partial fulfilment of the requirements for the degree of Master of Science.

ABSTRACT

The accuracy of the Moiré method for determining deflections and moments in laterally loaded thin plates has been well established in the literature. The main purpose of this thesis is to study whether or not the Moiré method can be applied to thermally loaded circular plates.

The following three axisymmetric problems have been investigated:-

1. Simply supported circular plate heated at the centre by an infrared heat lamp.
2. Clamped circular plate with the same heating as above.
3. Elastically supported circular plate with uniform heating around the edge.

For the first two cases experimental results have been compared with the existing theoretical results considering temperature gradients across the thickness only. There are no theoretical results available for the last case since the boundary conditions are arbitrary.

It appears that the Moiré method can be applied to determine the deflections and moments in thermally loaded thin metal plates. The results of the first two cases show that the deflection due to temperature gradient across the thickness of the plate is very small in comparison with the deflection contributed by radial temperature gradient for

the type of edge conditions simulated in the experiments. The accuracy of the Moiré method can not be assessed since theoretical analysis corresponding to the experimental situation is not available.

ACKNOWLEDGEMENTS

The author wishes to extend his appreciation to Dr. K.C. Cheng for his supervision of this thesis, to Dr. J.S. Kennedy for his helpful comments concerning the manuscript, and to Dr. D.G. Bellow for his advice on calibration of the plate material.

Thanks are extended to Dr. G. Ford for his guidance during the graduate studies at the University of Alberta.

Thanks are also extended to the staff of the Mechanical Engineering Shop for making the apparatus, particularly to Bill Kell and Andy Smart for their ready help during the experimental work.

He would also like to thank his wife, Darshan, for her encouragement and considerations.

TABLE OF CONTENTS

LIST OF TABLES

LIST OF FIGURES

LIST OF SYMBOLS

a = radius of circular plate

b = horizontal distance measured along the camera axis, from plate model to the grid

c = vertical distance measured from the camera axis to a point on the surface of the plate model

D = $\frac{Et^3}{12(1-\nu^2)}$, Flexural rigidity of a plate

d = pitch of lines on the grid

E = modules of elasticity

e = vertical distance measured from the camera axis of the point on the surface of the grid reflected to the photographic negative by a point R on the unloaded model

F = Airy's stress function

f = same as e, but for the loaded model

$H(r)$ = $\int_0^r \Theta \, r.dr$

L = horizontal distance measured along the camera axis, from plate model to the grid

M_r = radial bending moment per unit length

M_Θ = tangential bending moment per unit length

M_x, M_y = bending moments per unit length of sections of a plate perpendicular to the x and y axes, respectively

M_{xy} = twisting moment per unit length of a section of a plate perpendicular to x - axis

P = point load

q = uniform load

S = fringe spacing

T = temperature rise

$T_{D(o)}$ = temperature difference between the faces of the plate at the centre

$T_m = \frac{1}{t}\int_{-t/2}^{+\frac{t}{2}} T.dz$

T_{oa} = temperature difference between the edge and the centre of the plate

T_o = Initial plate temperature

t = plate thickness

w_{max} = Maximum deflection of a plate

(r,θ,z) = cylindrical polar coordinates

(u,v,w) = components of displacement

(x,y) = rectangular coordinates

α = coefficient of linear thermal expansion

Δ = f - e

$\nabla^2 = \left(\frac{\partial}{\partial r^2} + \frac{1}{r}\frac{\partial}{\partial r} + \frac{1}{r^2}\frac{\partial^2}{\partial \theta^2}\right)$ = Laplacian operator

$\Theta = \frac{12}{t^3}\int_{-\frac{t}{2}}^{+\frac{t}{2}} T.z.dz$

ν = Poisson's ratio

ϕ = change in slope

CHAPTER I

INTRODUCTION

1.1 Introduction

With the advent of space age, the problem of thermal stresses in thin plates became of great importance in the field of machine design. In this thesis axisymmetric thermal stresses in circular plates are investigated. The theoretical results available for such cases appear to be rather limited. In 1953, Goldberg [1]* presented the method of cuts to determine the radial and tangential bending moments in simply supported and clamped circular plates having constant thermal gradients across the thickness. Forray and Newman [2] gave expressions for deflections and bending moments in simply supported and clamped circular plates subjected to axisymmetric temperature distribution in the form of convergent power series. Boley and Weiner [3] and Flugge [4] gave expressions for the deflections and bending moments in simply supported and clamped circular plates under an axisymmetric temperature distribution.

Some experimental techniques are also available

---

* Numbers in brackets designate references at the end of thesis.

for the study of the thermal stresses in thin plates. Electrical resistance type strain-gauges have been used in the past to determine the thermal strains on the surface of metal plates. The use of the strain-gauge technique is somewhat involved at elevated temperatures, and entails large scale models and extensive heating facilities.

The photothermoelastic technique has been developed as an experimental approach to thermal stress problems. This technique extends the conventional photoelastic method of experimental stress analysis to the measurement and visualization of complete thermal stress fields arising from transient or steady state temperature gradients. This method was initiated by Gerrard and Gilbert [5]. They studied the thermal stresses in a free disk with a steel plug in the centre. The disk was subjected to a uniform temperature field. They also considered a beam with suddenly applied temperature differential on one edge. The plastic used was Paraplex P-43. Becker and Colao [6] studied the thermal stresses by the same method in rectangular, circular and hexagonal plates with free boundaries having uniaxial parabolic temperature distribution. In these investigations by photothermoelasticity the temperature gradients were established by refrigeration. This overcomes the problem of creep in plastics at elevated temperatures.

The Moiré method has been developed by Ligtenberg [7] to determine the deflections and moments in laterally loaded thin plates. Ligtenberg studied several laterally loaded thin plates and reported an accurracy of ±5 percent of the maximum moment, for the moments. Bradley [8] studied laterally loaded square plates with and without cutouts, both experimentally using the Moiré method, and analytically using finite differences. He found that the agreement between deflections and moments as found by the two methods was within 10 percent. Ligtenberg and Bradley used plastic models in these investigations. The possibility of using metal models was also discussed by them. One of the disadvantages of using plastic materials is that the modulus of elasticity varies with humidity and temperature. Tso [9] studied laterally loaded thin metal plates by the Moiré method. He found that the maximum error in comparison with theory was 6 percent for the deflections and 16 percent for the bending moments. Zienkiewicz and Cruz [10] performed some analogue experiments on laterally loaded thin plates in order to investigate the thermal stresses in thick tubes. They used Moiré method to determine the curvatures in the analogue experiments. Sciammarella and Ross [11] used the differential Moiré method to investigate the thermal stress problem in cylinders subjected to a symmetrical temperature distribution.

The main objective of this thesis is to investigate whether or not the Moiré method can be applied to the steady state thermal stress problem in thin metallic plates. The following three axisymmetric problems have been investigated:

1. Simply supported circular plate heated at the centre by an infrared heat lamp.
2. Clamped circular plate with the same heating as above.
3. Elastically supported circular plate with uniform heating around the edge.

The experimental and other details followed in this investigation are described in the following pages.

CHAPTER II

REVIEW OF THEORETICAL RESULTS

2.1 Governing thermoelastic plate equations.

Consider a circular plate of thickness, t. Any point in the plate may be defined by cylindrical polar co-ordinates (r, θ, z); the origin is taken at the centre of the plate in its middle plane.

The following are the governing thermoelastic plate equations for a circular plate subjected to a steady state temperature distribution [4] .

$$\nabla^2\nabla^2 F = Et\left\{\left[\frac{\partial}{\partial r}\left(\frac{1}{r}\frac{\partial w}{\partial \theta}\right)\right]^2 - \frac{\partial^2 w}{\partial r^2}\cdot\left(\frac{1}{r}\frac{\partial w}{\partial r}+\frac{1}{r^2}\frac{\partial^2 w}{\partial \theta^2}\right) - \alpha\nabla^2 T_m\right\} \tag{1.a}$$

$$D\nabla^2\nabla^2 w = \left(\frac{1}{r}\frac{\partial F}{\partial r}+\frac{1}{r^2}\frac{\partial^2 F}{\partial \theta^2}\right)\cdot\frac{\partial^2 w}{\partial r^2} - 2\frac{\partial}{\partial r}\left(\frac{1}{r}\frac{\partial F}{\partial \theta}\right)\cdot\frac{\partial}{\partial r}\left(\frac{1}{r}\frac{\partial w}{\partial \theta}\right)$$

$$+ \frac{\partial^2 F}{\partial r^2}\left(\frac{1}{r}\frac{\partial w}{\partial r}+\frac{1}{r^2}\frac{\partial^2 w}{\partial \theta^2}\right) - (1+\nu)\,D\alpha\nabla^2\Theta \tag{1.b}$$

where,

$\nabla^2 = \left(\frac{\partial^2}{\partial r^2}+\frac{1}{r}\frac{\partial}{\partial r}+\frac{1}{r^2}\frac{\partial^2}{\partial \theta^2}\right)$ = Laplacian operator,

F = Airy's Stress Function,

$$T_m = \frac{1}{t}\int_{-\frac{t}{2}}^{+\frac{t}{2}} T.dz,$$

$$\Theta = \frac{12}{t^3}\int_{-\frac{t}{2}}^{+\frac{t}{2}} T.z.dz.$$

These equations are based on the following assumptions:

(i) The plate is in a state of plane stress.

(ii) The deformations of the plate due to shearing stresses are neglected.

(iii) The plate constants E, ν and α are independent of temperature.

The differential equations 1.(a) and 1.(b) are non-linear, and their general solutions are not available. They are, as noted in [4] restricted to small displacements u and v but deflection w can be finite. If w is also small, the non-linear terms may be neglected, giving

$$\nabla^2\nabla^2 F = -Et\alpha\nabla^2 T_m \qquad (2.a)$$

$$\nabla^2\nabla^2 w = -(1+\nu)\,\alpha\nabla^2\Theta \qquad (2.b)$$

For a circular plate, in which the temperature varies across the thickness and along the radius, but is independent of the polar angle θ, the general solution of equation 2.(b) is given by [4] ,

$$w = (1+\nu)\,\alpha\left[c_1 + c_2 r^2 + \int_r^a \frac{H(r)}{r}\,.\,dr\right] \qquad (3)$$

where, $H(r) = \int_o^r \Theta r\,.\,dr$

The bending moments are given by [4] ,

$$M_r = -D\left[\frac{d^2w}{dr^2} + \frac{\nu}{r}\frac{dw}{dr} + (1+\nu)\,\alpha\Theta\right] \quad \text{and} \qquad (4.a)$$

$$M_\theta = -D\left[\frac{1}{r}\frac{dw}{dr} + \nu\frac{d^2w}{dr^2} + (1+\nu)\,\alpha\Theta\right] \qquad (4.b)$$

Substituting for w in the above equations,

$$M_r = -(1+\nu)\,\alpha D\left[2(1+\nu)c_2 + \frac{1-\nu}{r^2}H(r)\right] \quad \text{and} \qquad (5.a)$$

$$M_\theta = -(1+\nu)\,\alpha D\left[2(1+\nu)c_2 - \frac{1-\nu}{r^2}H(r) + (1-\nu)\Theta\right] \qquad (5.b)$$

The constants c_1 and c_2 are determined from the boundary conditions as follows:

a) Simply supported circular plate.

Since the boundary conditions are $w = 0$ and $M_r = 0$ along the edge at $r = a$, it follows that

$$c_1 = -a^2c_2 = \frac{1-\nu}{2(1+\nu)}\,H(a).$$

b) Clamped circular plate.

Since the boundary conditions are $w = 0$ and $\frac{dw}{dr} = 0$ along the edge at $r = a$, it follows that

$$c_1 = -a^2c_2 = -\frac{1}{2}H(a).$$

Let $T_{1(r)}$ and $T_{2(r)}$ be the temperatures at the points $(r,\theta,\pm\frac{t}{2})$. Provided $T_{1(r)} - T_{2(r)}$ is small the thermal conductivity may be assumed constant, so the thermal gradients across the thickness are constant. The temperature rise T at any point (r,θ,z) in the plate is then

given by,

$$T = \frac{1}{2}\left[T_{1(r)} + T_{2(r)}\right] + \frac{z}{t}\left[T_{1(r)} - T_{2(r)}\right] - T_o \qquad (6)$$

where, $T_{1(r)} > T_{2(r)}$.

The foregoing solution for the deflection given by equation (3), does not (as was pointed out by Goodier [12]) take into account the effects of the term $\left\{\frac{1}{2}\left[T_{1(r)}+T_{2(r)}\right] - T_o\right\}$, which is independent of z. This term represents a radial temperature distribution, which would introduce membrane forces in the plate if the plate were constrained from radial movement at the edge. The survey of literature shows that as yet there is no solution available which takes into account these radial thermal gradients. No attempt was made in this thesis to obtain such a solution.

CHAPTER III

EXPERIMENTAL APPARATUS AND PROCEDURE

3.1 The Moiré Method.

The Moiré method provides the slopes at all points on the plate model. Knowing the slopes the curvatures and deflections can be computed. From the knowledge of curvatures the bending moments can be determined in the plate model. The principles of Moiré method were fully explained by Ligtenberg [7] and Bradley [13] . They are briefly reviewed here for completeness.

The essential elements of the Moiré apparatus consist of the plate model having a reflecting surface, a fine lined grid of alternate black and white lines of equal width, and the camera, mounted behind a small hole in the screen, as shown in Fig. 1. The grid is illuminated with four photoflood lamps. The distance, L, from the plate model to the grid was 25 in. And the distance, b, from the plate model to the lens of the camera was 26.25 in. (i.e. $b = 1.05L$). Further details of this apparatus are given in reference [9] . The test set up is shown in Figs. 2(a) and 2(b).

The slopes are determined by first taking a photograph of the image of the grid reflected by the unloaded plate model, and then photographing on the same negative the image of the grid reflected by the loaded plate model.

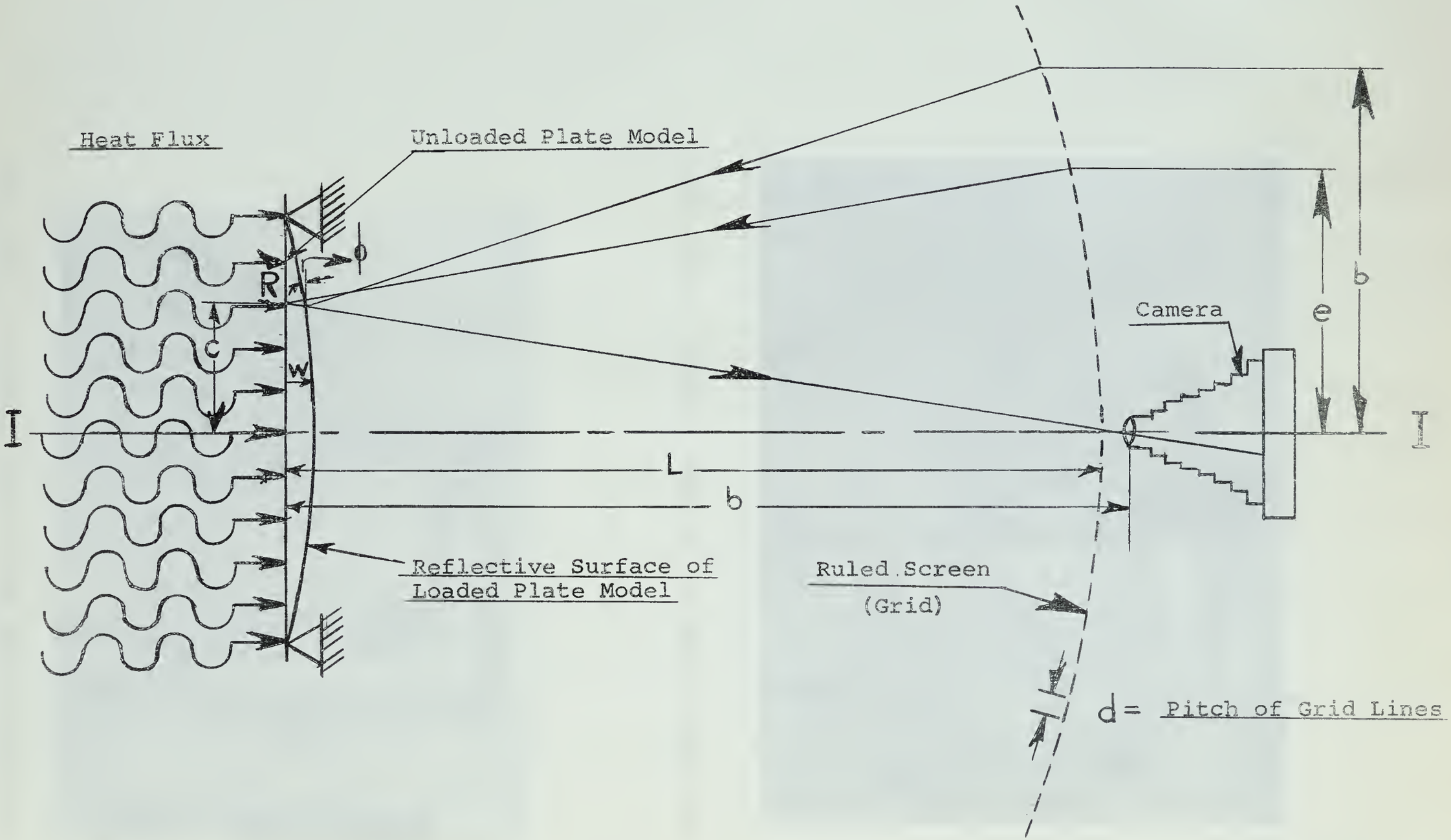

Fig. 1. Schematic diagram for Moiré Principle.

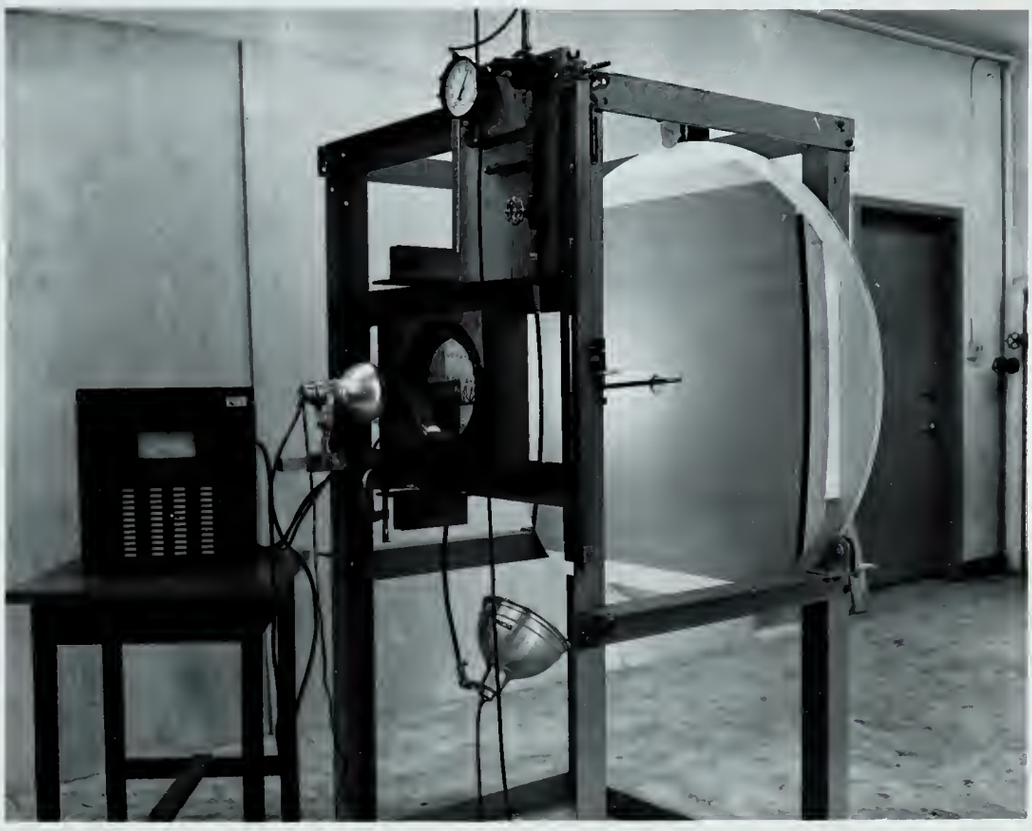

Fig. 2(a). General view of the Moiré Apparatus.

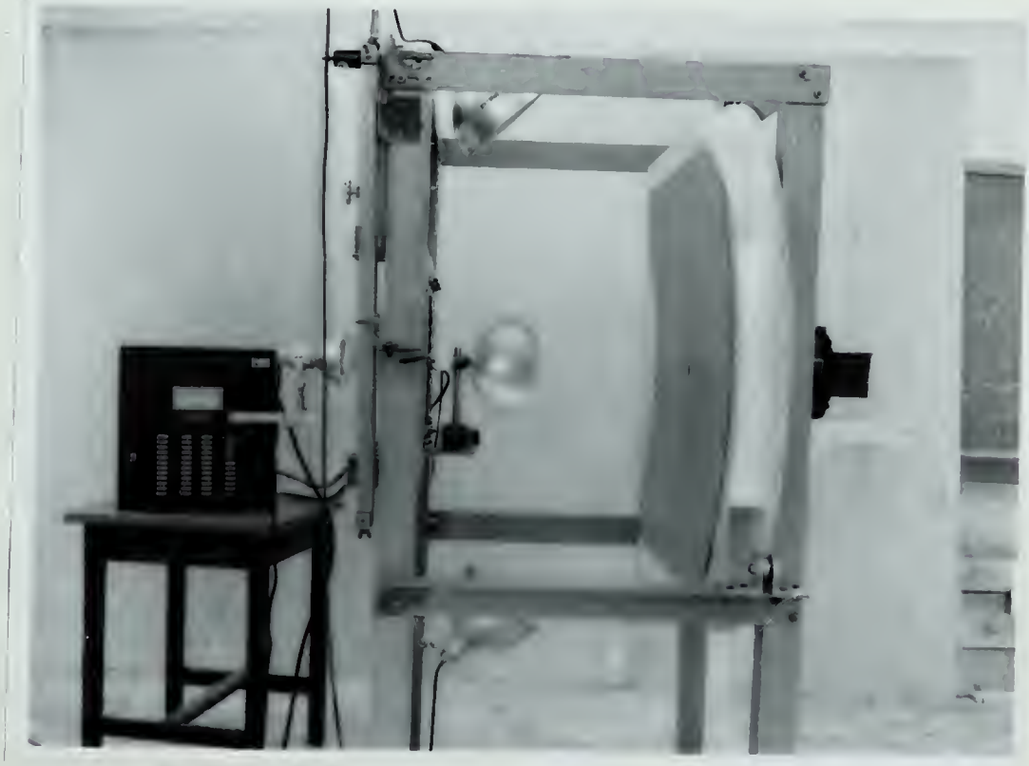

Fig. 2(b). General view of the Moiré Apparatus.

The interference of the two images produces Moiré fringes. These fringes can be interpreted as contour lines for the slopes. The change in slope, Φ, at any point R, on the plate model, from the unloaded condition to the loaded condition is determined by finding the difference (Δ) between distances f and e (as shown in Fig. 1). e is the distance from the axis I-I to the point on the surface of the grid reflected to the photographic negative by the point R on the unloaded model. f is the distance from the axis I-I to the point on the surface of the grid reflected by the same point R on the loaded model.
For a curved screen it can be shown that [7,13] ,

$$\Delta = f - e = 2L\Phi$$

The Moiré fringes on the print will result in a series of light regions and other regions in which the original grid appears. The change in slope Φ, for the plate model in going from one fringe to the neighbouring fringe is given by, $\Phi = \frac{d}{2L}$ [7,13] . For the apparatus used the change in slope between the neighbouring fringes is 0.002, i.e. $\frac{d}{2L}$.

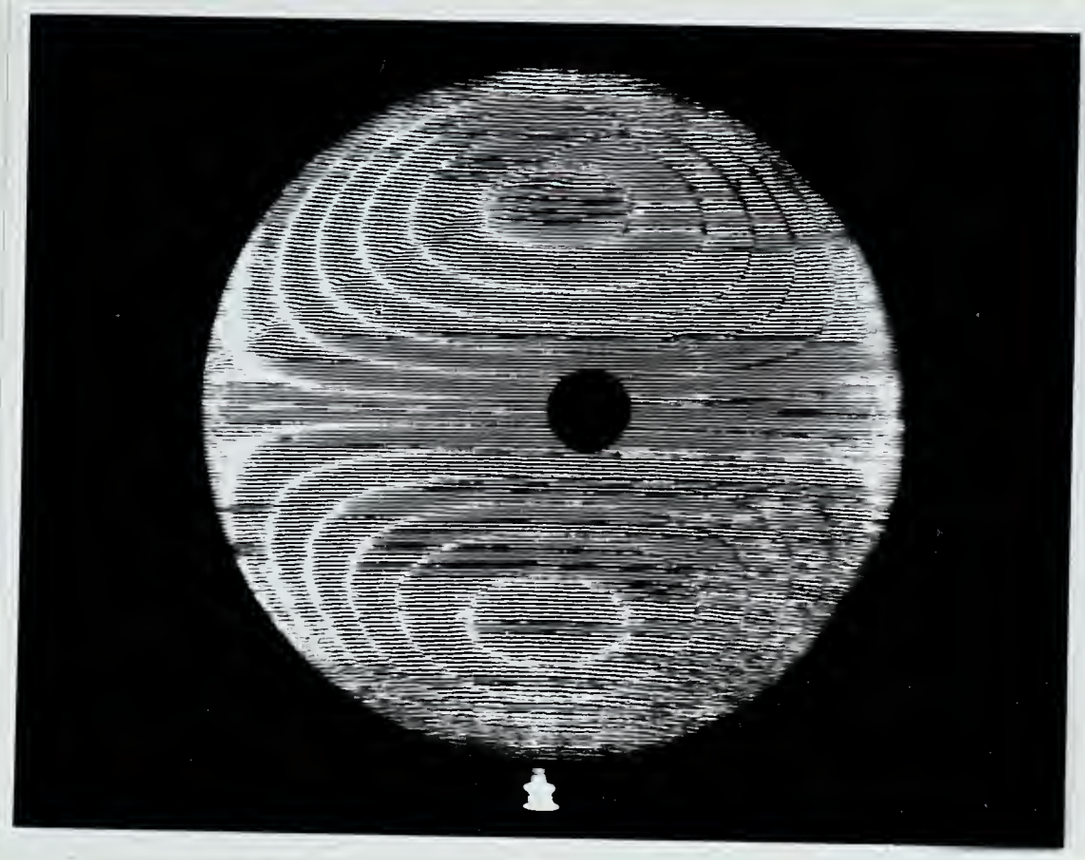

Fig. 3. Moiré Fringe Pattern for the Clamped Circular Plate, with Uniform Loading, $q = 6.44$ lb/in.^{2} Brass plate, thickness = 0.0907 in., diameter = 9.0 in., Maximum Deflection, $w_{max} = 0.03458$ in.

For example, Fig. 3 represents the Moiré fringes for the clamped circular plate with uniform loading. This picture was taken with the grid direction being horizontal. From these fringes the slopes of the plate model along its vertical diameter can be determined. Since the edge of this plate is clamped, the slope in the radial direction at the edge is zero. In this picture the fringes are of zero order at the ends of the vertical diameter. From symmetry the slope is also zero at the centre of the plate. With this information these Moiré fringes can be analysed

and the slope versus radius curve can be drawn for this plate. The deflections are found by integrating the area under the slope versus radius curve. The curvatures are computed by taking the slopes of the slope versus radius curve.

3.2 The Apparatus.

a) Model Supports.

The plate model tested was held in a vertical position in the test frame. In this investigation, simply supported, clamped and elastically supported circular plates were studied.

For the simply supported circular plate, two 1 in. thick steel plates were machined as shown in Fig. 4(a). The plate model was supported on the knife edges, on both faces. The assembly was drawn together by barely tightening the twelve 1/2 in. bolts. The tip of the knife edge was about 1/64 in. thick, having an inner diameter of 9.078 in.

For the clamped circular plate, two 1 in. thick steel plates were machined as shown in Fig. 4(b). The assembly was clamped together by twenty-four 1/2 in. bolts. The bolts were gradually tightened to a torque of 70 ft-lb. using a torque wrench, to achieve the clamped boundary conditions. The inner diameter of the support steel plates was 9 in.

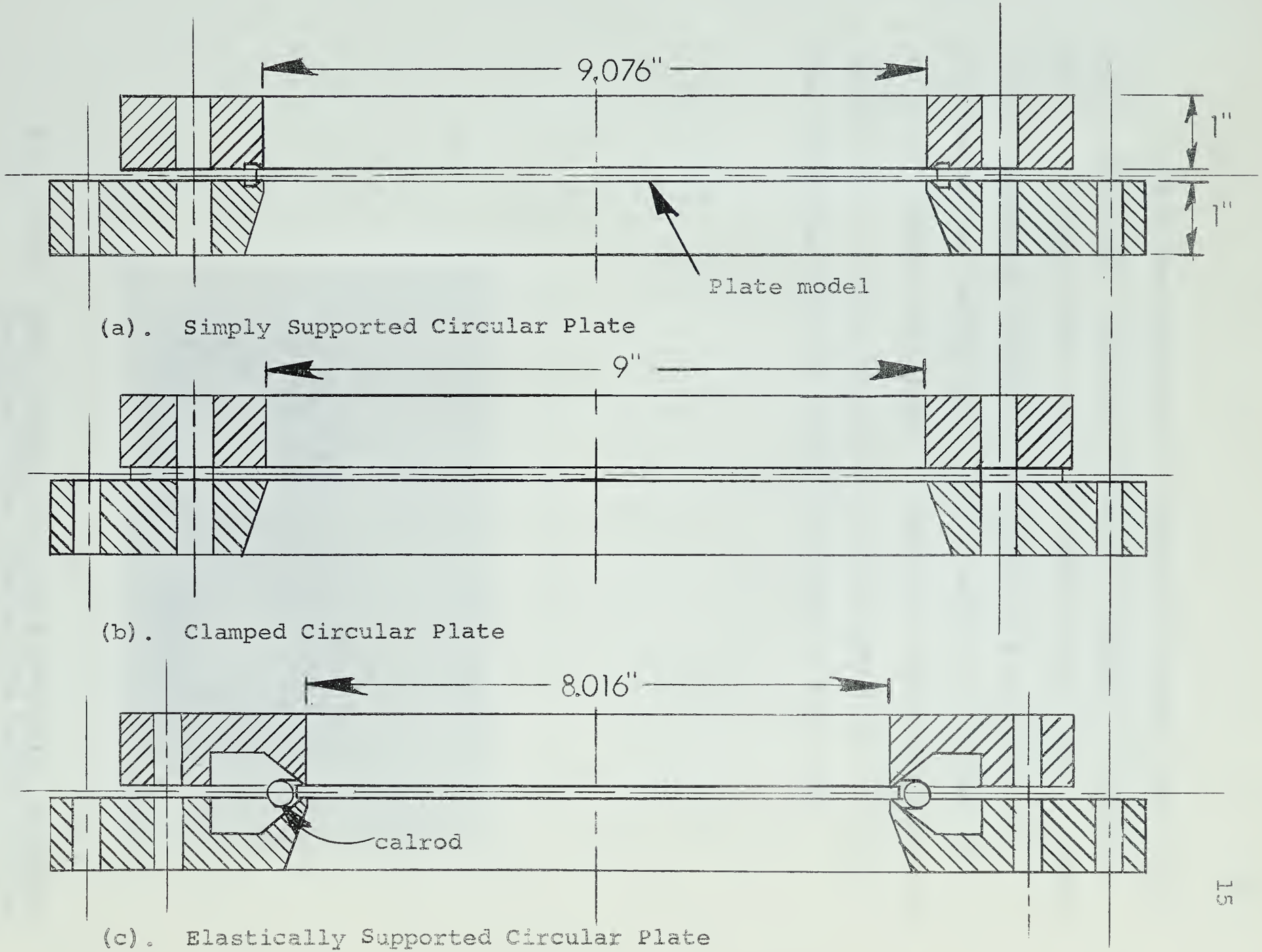

Fig. 4. Sectional Views for the Assemblies.

For the elastically supported circular plate, the plate model was supported on the knife edges, in between two 1 in. thick steel plates as shown in Fig. 4(c). Elastically supported boundary conditions were achieved, by tightening the twenty-four 3/8 in. bolts to a torque of 40 in-lb. torque each time. The tip of the knife edge was about 1/64 in. thick having an inner diameter of 8.016 in. The insulation and the calrod are shown in Fig. 4(d).

Fig. 4(d). Model Support for the Elastically Supported Circular Plate, showing the Calrod and the Insulation.

b) The model.

In this investigation, ALCLAD 7075-T6, QQ-A-287A ALCOA, 0.063 in. thick aluminum sheet was used. One face of the plate model was polished with silvo polish. The plate model was polished to such an extent that the image of the grid at a distance of 25 in. away could be seen clearly.

c) Heating arrangement for the plates.

The simply supported and clamped circular plates were heated at the centre from one face, with a General Electric 250 watts infrared heat lamp, having a built-in reflector. The infrared heat lamp was mounted concentrically with the central axis of the plates, on a square steel bar fixed to the model support as shown in Fig. 5. The lamp was mounted so that it could be positioned along this bar. The steel bar was engraved with 1/16 in. marks to facilitate the measurement of distance between the lamp and the plate. The heat flux was controlled by varying the distance between the lamp and the plate. The plate was heated from one face mostly by thermal radiation and partly by free convection. The plate lost heat into the atmosphere on the other face by free convection. Some heat was also lost by conduction at the plate edge. It was possible to create stable thermal gradients across the thickness and along the radius of the plate by heating it in this manner.

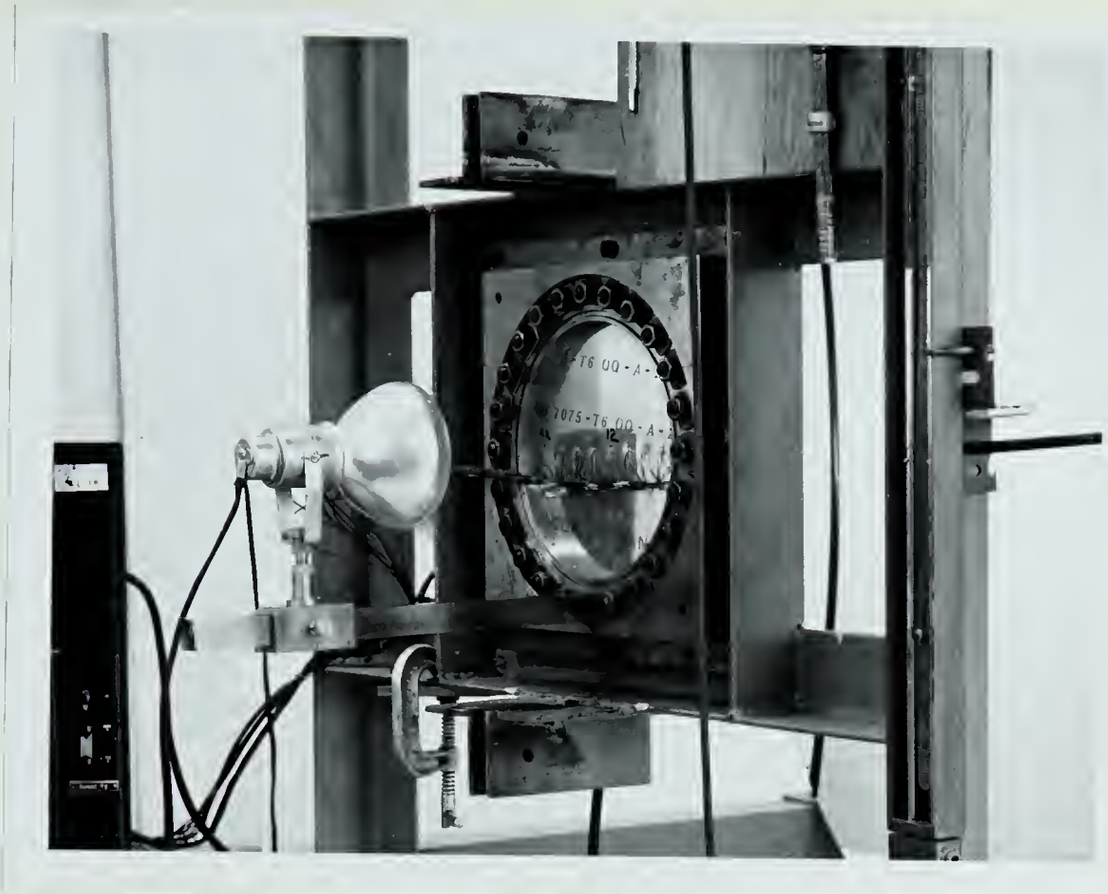

Fig. 5. Fixture for the Infrared Heat Lamp.

The elastically supported circular plate was heated at the edge, by means of a calrod, such that there were no thermal gradients across the thickness of the plate. Uniform heating across the thickness of the plate was achieved, by centering the calrod with the middle plane of the plate. A 0.315 in. diameter circular cross-section, 38 in. long, 1000 watts steel calrod was bent into a circle of 8 1/4 in. inner diameter, to surround the edge of the plate. The bent calrod was fixed to the bottom support steel plate by means of six clamps. The support steel plates were insulated from the calrod by an

asbestos insulation. The plate was heated at the edge by thermal radiation and free convection, and it lost heat into the atmosphere from both faces by free convection. Probably there was also some heat loss at the knife edge due to conduction. The heat output from the calrod was controlled by a variac.

In this investigation, only the heating apparatus and the model support for the elastically supported circular plate were constructed. All the rest of testing apparatus was already available in the mechanical engineering laboratory.

3.3. Temperature and its measurement.

In this investigation the temperatures were measured by thermocouples. Honeywell Type-J iron-constantan thermocouple wires were used. The thermocouples were spot welded along the horizontal diameter on both faces of the plate, as shown in Fig. 6. The thermocouples were spot welded one inch apart starting from the centre of the plate, and the end thermocouples were 1/4 in. away from the boundary of the plate. The exact location of thermocouples along the diametric sections of the plates are shown in Figs. 7(a) and 7(b).

Fig. 6. Spot welded Thermocouples on the 9 in. diameter, Clamped Circular Plate.

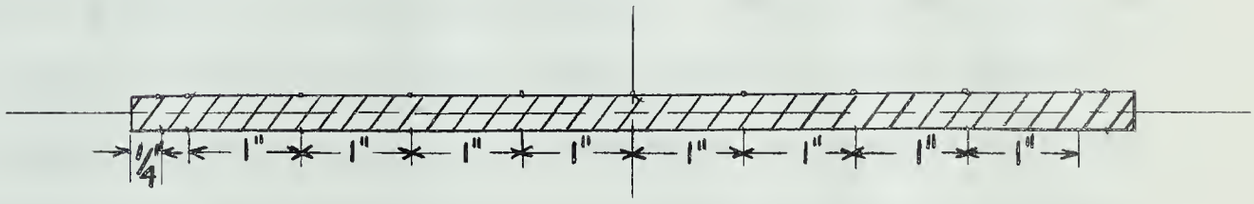

Fig. 7(a). Diametric Section of the Plate, showing the Location of Thermocouples for the Simply Supported and Clamped Circular Plates.

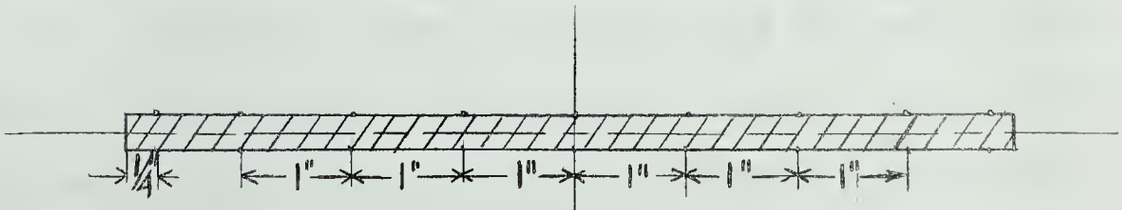

Fig. 7(b) Diametric Section of the Plate, showing the Location of Thermocouples for the Elastically Supported Circular Plate.

a) Preparation and spot welding of thermocouples.

To make the thermocouple junction, the ends of both wires were cleaned with fine emery cloth. They were then twisted together, and cleaned by dipping into carbon-tetrachloride. The thermocouple junctions were then held on to the plate by black adhesive tape. Then they were spot welded to the plate. Care was taken to ensure that the twist of the thermocouple wires terminated at the point where spot welding was done, and to see the thermocouple wires were not in contact with each other, or with the plate, beyond the spot welded junction.

The plate model and the thermocouples were held between the electrodes of the spot welder, as shown in Fig. 8. On passing current through the electrodes, the two thermocouples were simultaneously spot welded on opposite points of the plate model. The spot welding was done using a Miller portable spot welder, model LMSW5Z. This spot welder is primarily designed to operate on 250 volts, but it was operated on 110 volts, and the current was passed for 2 1/2 seconds to make each weld.

b) Calibration of the thermocouples.

Two different sizes, 24 gauge and 30 gauge Honeywell Type-J iron-constantan wires were used to measure the temperatures. The 24 gauge wire was used for the plate model with clamped boundary conditions, and the 30 gauge wire was used for the other two cases.

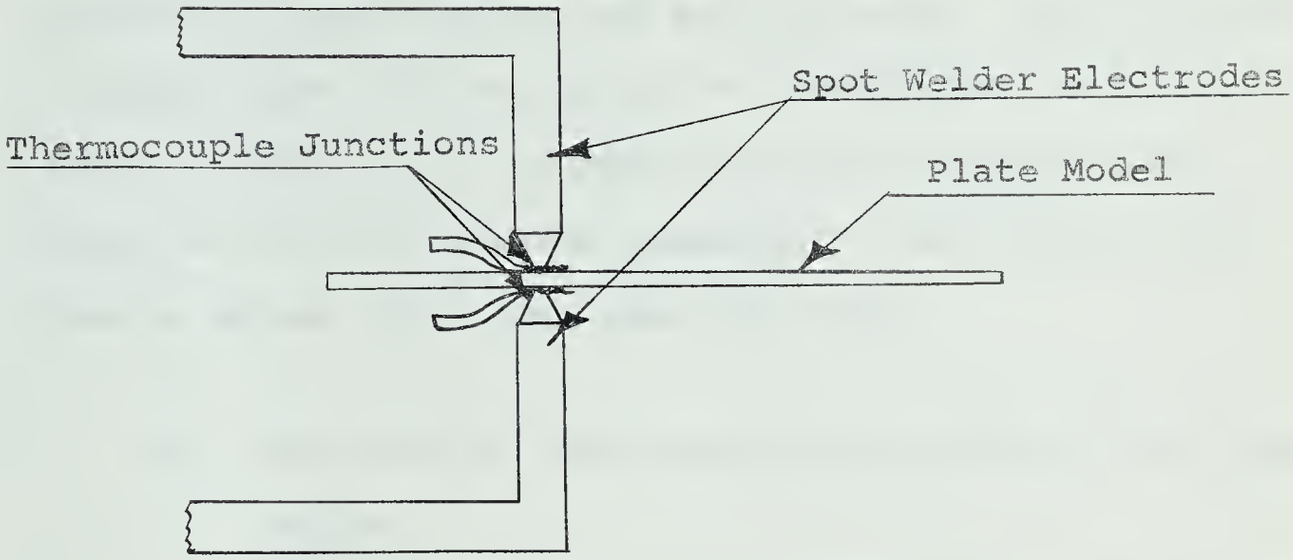

Fig. 8. Spot welding arrangement, showing the Spot Welder Electrodes, Thermocouple Wires and the Plate Model.

Six thermocouple junctions were made and spot welded on a 2 x 3 x 0.063 in. aluminum strip. This aluminum strip was immersed in a mixture of melting ice and water, and then in boiling water. The temperature readings from the recorder were compared with the temperature readings from a mercury thermometer. For any one bath these thermocouples gave the same reading. This procedure was done for both (24 and 30 gauge) wires separately. The temperature readings from the recorder and the thermometer were in good agreement, for the melting

ice and boiling water, for the 30 gauge wire. For the 24 gauge wire the recorder gave lower readings of temperature for melting ice and boiling water. The recorder readings were 2°F less than the thermometer readings. Thus, in the case of clamped circular plate 2°F were added to all the recorder readings. The thicker wire gave a better joint than the thin wire.

c) Recording of the temperature readings from thermocouples.

The temperatures were recorded by means of Honeywell Brown Electronic temperature recorder. This recorder is designed to read 36 Type-J thermocouple wires and 6 Type-F thermocouple wires. The temperatures were read directly in degrees Fahrenheit on a circular scale, which was activated by pressing a push-button for each thermocouple. It was possible to read this circular scale within $\pm$ 1/4°F for each temperature reading.

d) Axial symmetry of temperature distribution.

In the case of simply supported and clamped circular plates, axially symmetric temperature distribution was achieved by lining up the centre of the plate with the centre of the infrared heat lamp. The axial symmetry of temperature distribution was checked by two methods:

1. By rotating the infrared heat lamp about its own axis.

The plate was heated for four different angular pos-

itions of the infrared heat lamp. The corresponding readings of thermocouples were in good agreement for all the four positions. This proves symmetrical temperature distribution.

2. By checking the Moiré fringe patterns for the different directions of the grid.

The plate was heated and similar Moiré fringe patterns were produced for 0°, 45°, 90° and 135° grid directions. The grid directions are shown in Fig. 9. This similarity in Moiré fringe patterns shows that the plate deflected symmetrically with respect to its centre.

In the case of the elastically supported circular plate, the plate was heated at the edge, and similar Moiré fringe patterns were produced for 0°, 45°, 90°, and 135° grid directions. The results showed that the plate deflections were axisymmetric.

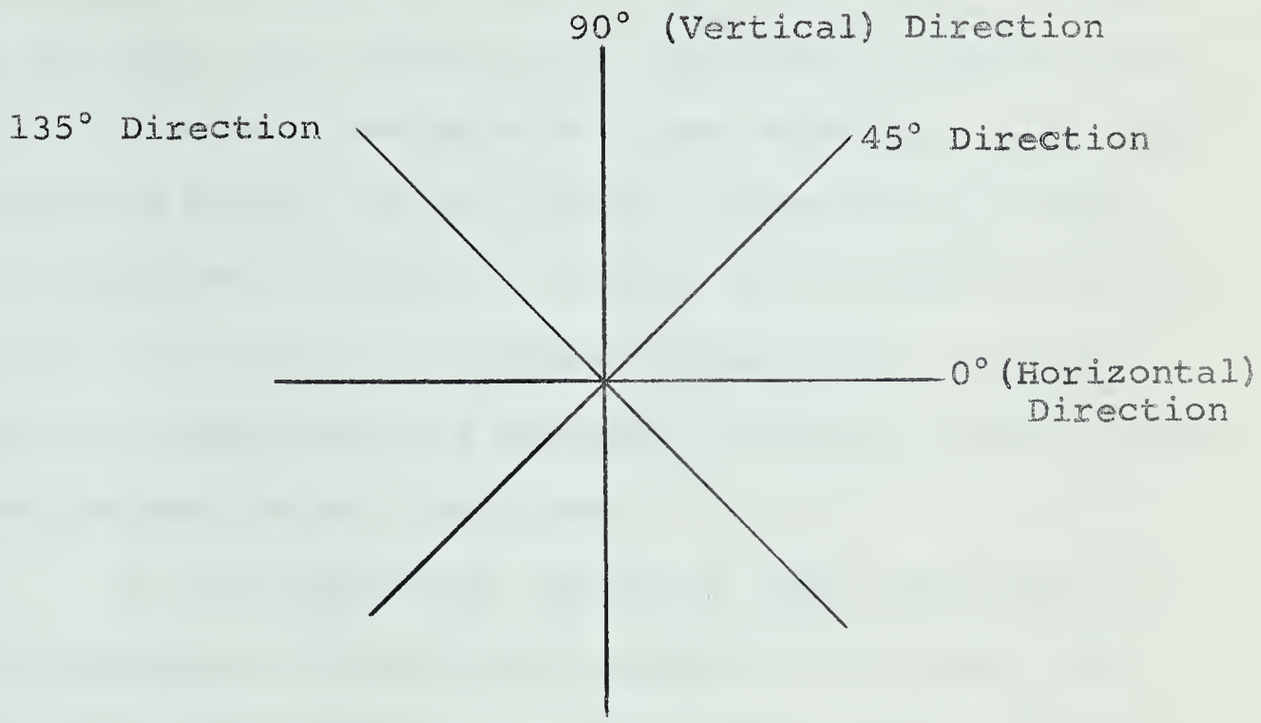

Fig. 9. Grid Directions for the Tests.

3.4 Test Procedure.

The well polished plate model, with thermocouples spot welded along the horizontal diameter on both faces, was placed in the test frame. Then the first exposure was made for the 0° (horizontal) grid direction. The plate was then heated very slowly, and the deflection was measured near the centre of the plate by a dial gauge. This provided a check on the maximum deflection of the plate. The heating of the plate was controlled to ensure that the maximum deflection of the plate was less than half the thickness of the plate. The temperature and deflection

became quite steady after about two hours, after which the dial gauge was removed and the second exposure was made. Then the grid was rotated to 90° (vertical) direction and the first exposure was made on a new negative. The plate was allowed to cool to its initial temperature and the second exposure was made. It took six to seven hours for the plate to cool to its initial temperature. In this manner two negatives were produced, exhibiting Moiré fringes in two perpendicular directions.

It was originally planned to test one model as simply supported and uniformly heated at the edge. On testing it was found that for the simple support boundary conditions the plate model did not deflect enough to give sufficient Moiré fringes. To increase the deflection, an attempt was made to achieve clamped boundary conditions by tightening the bolts of the model support. An examination of the Moiré fringes for this case showed that it was not possible to obtain clamped boundary conditions with this support. Since this model could not be tested as simply supported or clamped, it was decided to test it as an elastically supported circular plate. This was done by tightening the twenty-four model support bolts to a torque of 40 in-lb each, in increments of 5 in-lb torque. While tightening these bolts to 40 in-lb, the plate model deflected 0.045 in. at the centre. This deflection was checked by

a dial gauge and the Moiré fringe analysis. The plate model with this initial curvature was then heated. The maximum deflection was of the order of 0.038 in. For this case, two tests were run, and the Moiré fringe patterns were produced for 0° and 90°, and 45° and 135° grid directions.

The photographs were enlarged to full size, on Kodak Kodabromide, light weight, A.5, photographic paper. The Moiré fringes were traced and analysed. Knowing the slopes and curvatures from Moiré fringes, the bending moments were computed from equations (4). The deflections were computed by integrating the area under the slope versus radius curve.

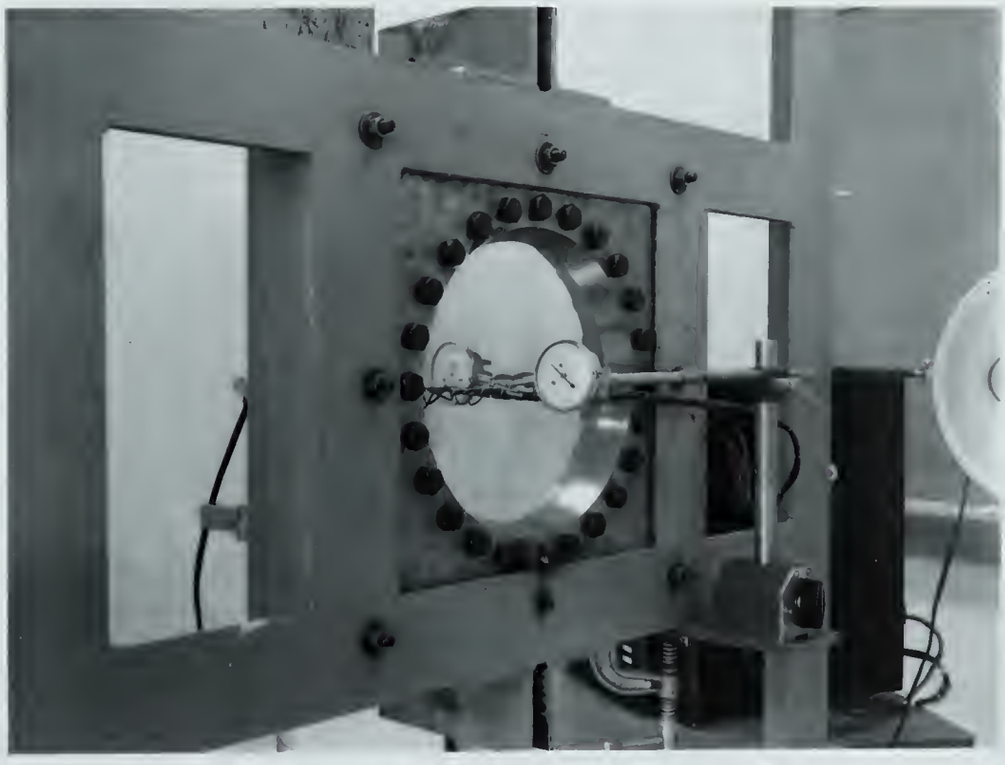

Fig. 10. View showing the Dial Gauge, measuring the Maximum Deflection of the Plate Model.

3.5 Calibration of the material.

Originally it was planned to study the thermal stresses in 0.0907 in. thick half hardened yellow brass plates. This material was calibrated to determine its modulus of elasticity, E, and Poisson's ratio, ν. After this calibration, the simply supported and clamped circular plates were heated with a 375 watts infrared heat lamp. It was found that the heat output from this lamp was not sufficient to deflect these plates. The study was therefore switched over to 0.063 in. thick aluminum plates. The value of the bending rigidity, D, for aluminum plates was taken from reference [9] .

Three methods for the calibration of the brass plate were used and are discussed below:

a) Clamped circular plate with uniform loading.

For a uniformly loaded clamped circular plate of radius, a, the centre deflection is [14] ,

$$w_{max} = \frac{qa^4}{64D} \tag{7}$$

Thus, after loading the plate and measuring the centre deflection, the plate rigidity, D, can be computed. The clamped circular plate was loaded by air pressure applied through a steel air box. The air pressure was measured by a mercury manometer. The centre deflection was measured by a dial gauge, and was checked by Moiré fringe analysis

for this loading (see Fig. 3). For $q = 6.44$ lb/in^2 the centre deflection was 0.03458 in., from the Moiré fringe analysis. From these values, the value of D for brass plate was found to be 1193 in-lb.

As an additional check a graph was plotted between the centre deflection, w_{max}, and the uniform loading, q, as shown in Fig. 11. From this graph $\frac{w_{max}}{q} = 5.33 \times 10^3$ in^3/lb and this gave the value of D for brass a 1202 in-lb.

b) Square plate simply supported at three corners and loaded with a concentrated load, P, at the fourth corner.

A 6 x 6 in. square plate was simply supported at three corners and loaded by a point load at the fourth corner. The x and y axes were taken along the diagonals as indicated in Fig. 12(b). Then M_x, M_y and M_{xy} were constant throughout the plate [7,14].

The bending rigidity, D is given by [7, 13],

$$D = \frac{PS}{2(1-\nu)(\frac{d}{2L})} \qquad (8)$$

In this test Moiré fringes were produced for three different values of P and average S computed for each loading. Knowing d, L, and ν (which are constants), the applied load, P, and fringe spacing, S, the bending rigidity, D, was computed from equation (8). The respective values of P,

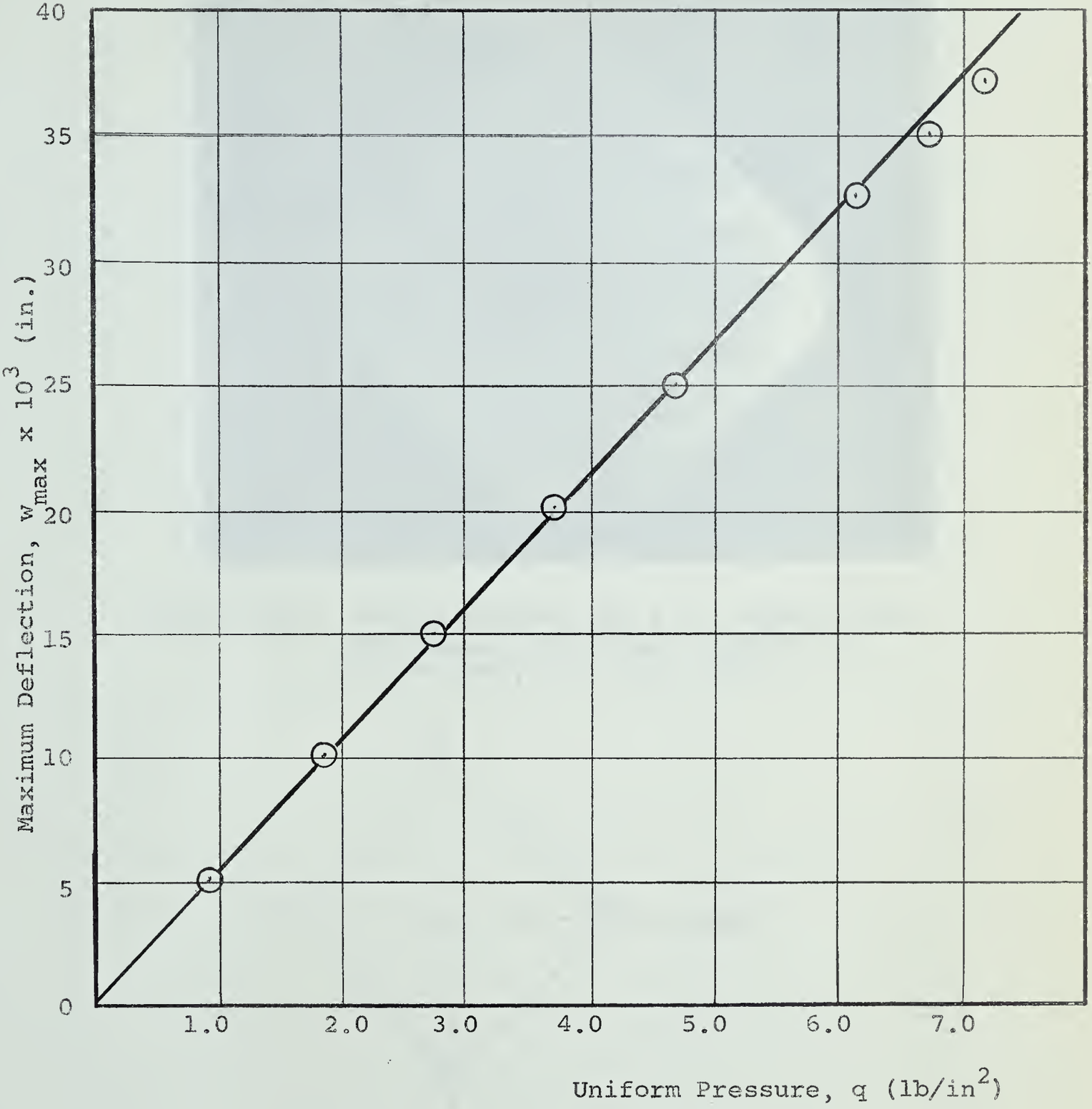

Fig. 11. Maximum Deflection versus Uniform Pressure, q, for the Clamped Circular Plate.

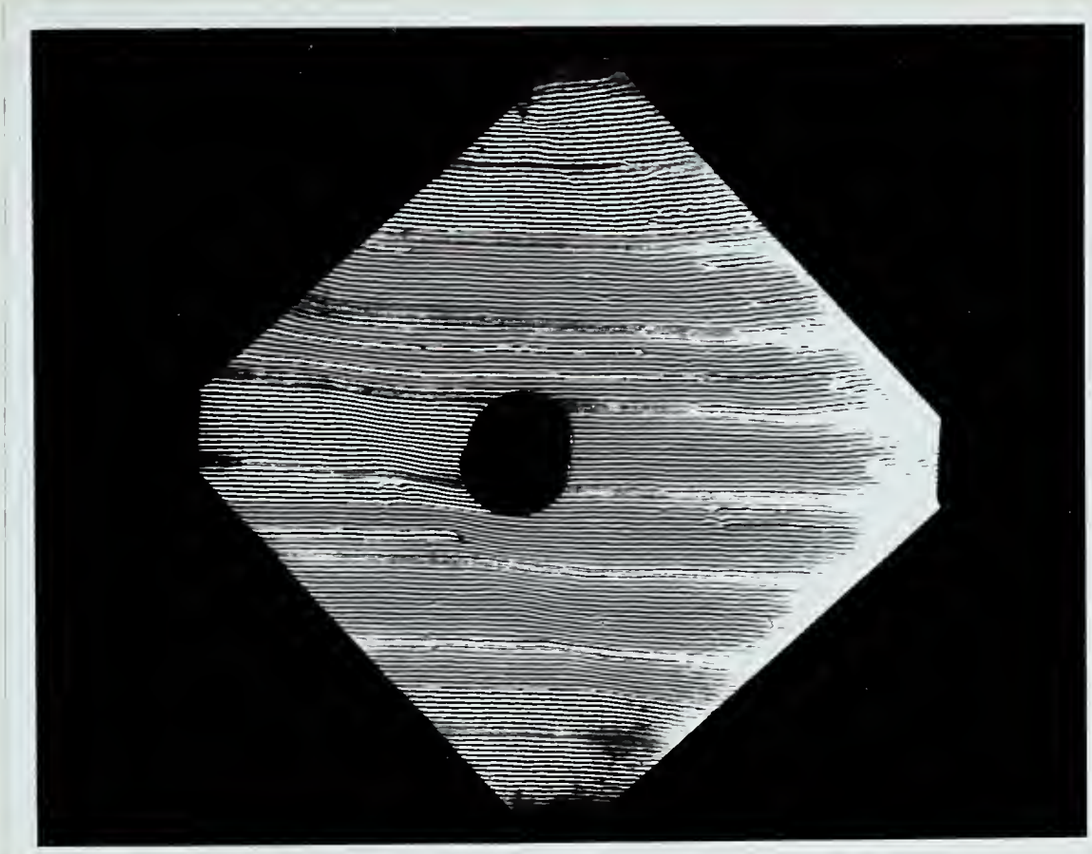

Fig. 12(a). Fringe Pattern for 6 in. Square Plate of brass. Thickness = 0.0907 in., Point load, P = 3.8 lbs.

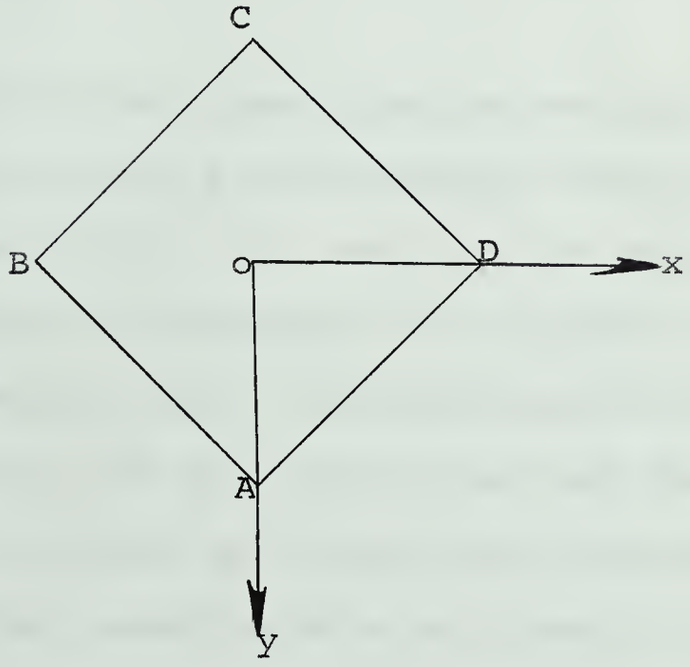

Fig. 12(b). Square Plate Simply Supported at B, A and D. Load P applied at C.

number of fringes, average S and D are tabulated in Table I for the three loadings.

Table I. VALUES OF D, AVERAGE S, NUMBER OF FRINGES AND LOAD, P, FOR THE 6 x 6 IN. BRASS SQUARE PLATE.

Point load, P (lb)	Number of fringes	Average S	$D = \frac{PS}{2(1-\nu)\frac{d}{2L}}$ (in-lb)
2.9	8	1.09	1198
3.4	9	0.943	1212
3.8	10	0.831	1198

c) Tensile Test.

This is a fairly simple and very reliable method for determining the modulus of elasticity, E, and Poisson's ratio, ν.

A 24 x 2 in. brass specimen was cut, and two 1/4 in. Budd metalfilm C6-141-B strain-gauges were mounted on its faces as shown in Fig. 13. The specimen was held in the testing machine, by clamping 6 in. lengths on each end in the testing machine jaws. The specimen was loaded in the testing machine, and the longitudinal and the transverse strains were recorded on a BLH strain indicator. This BLH strain indicator gave the strains directly in micro inch per inch. A maximum load of 3,000 lbs. was applied in

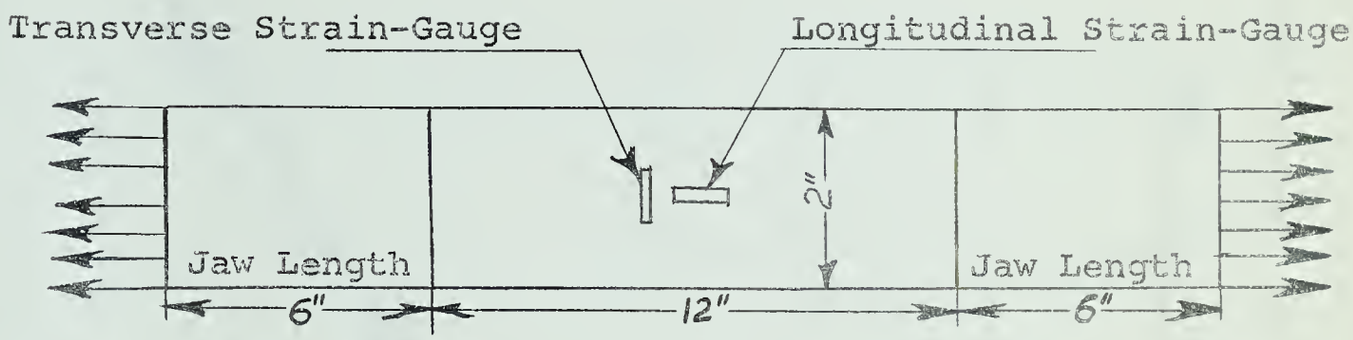

Fig. 13. Brass Specimen for the Tensile Test.

increments of 500 lbs.

The specimen was loaded first, and then unloaded and again loaded. This gave three sets of readings. Average longitudinal and transverse strains were calculated for the specimen, by averaging the strains for both faces of the specimen.

Stresses versus longitudinal strains were plotted, in Fig. 14, to compute the modulus of elasticity, E. Longitudinal strains versus transverse strains were plotted, in Fig. 15, to determine Poisson's ratio, ν. This gave, $E = 16.6$ lb/in.^{2} and $\nu = 0.34$. The value of bending rigidity, D, based on these values of E and ν was found to be 1210 in-lb.

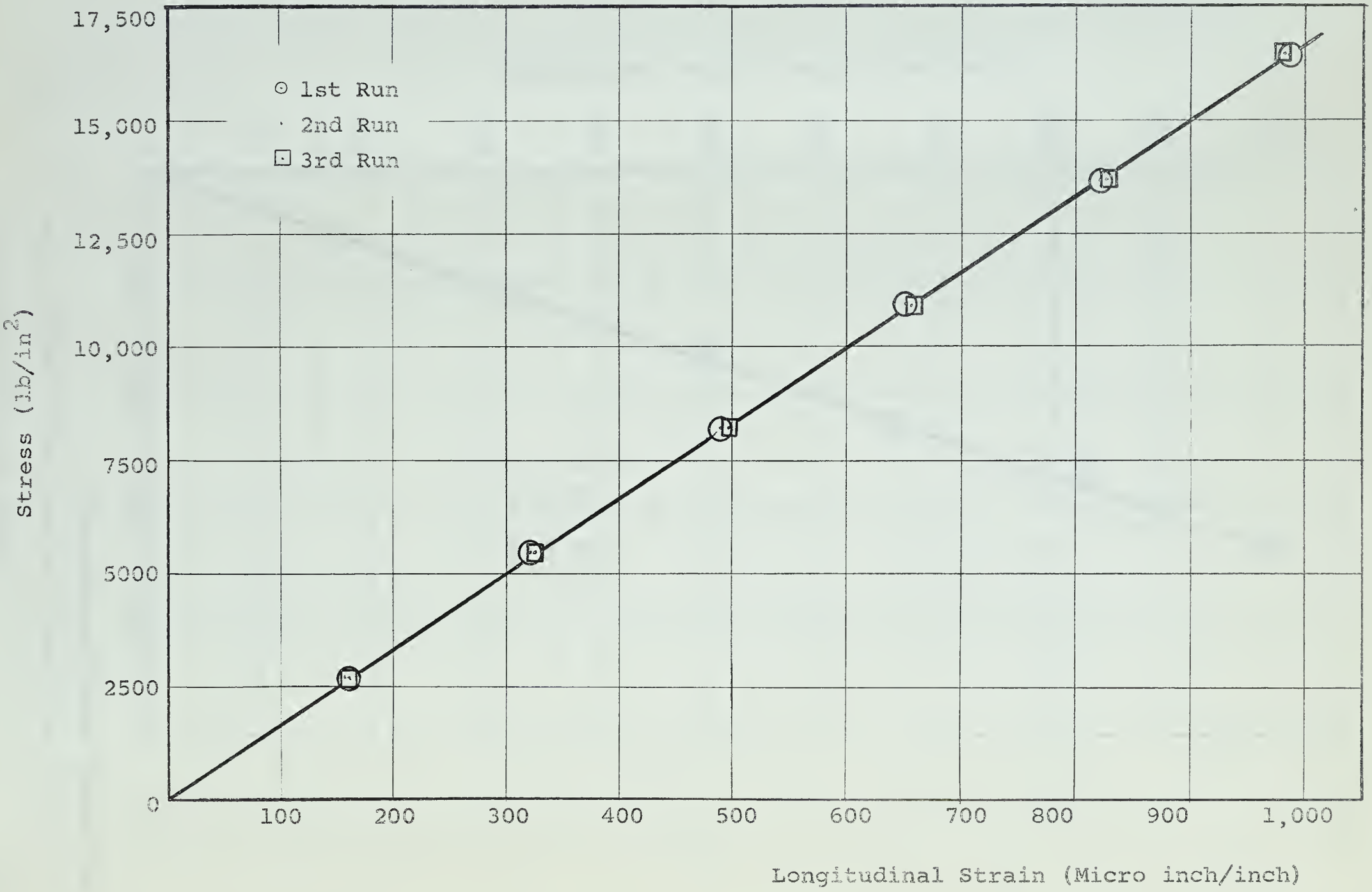

Fig. 14. Stress versus Longitudinal Strain for Tensile Test on Brass.

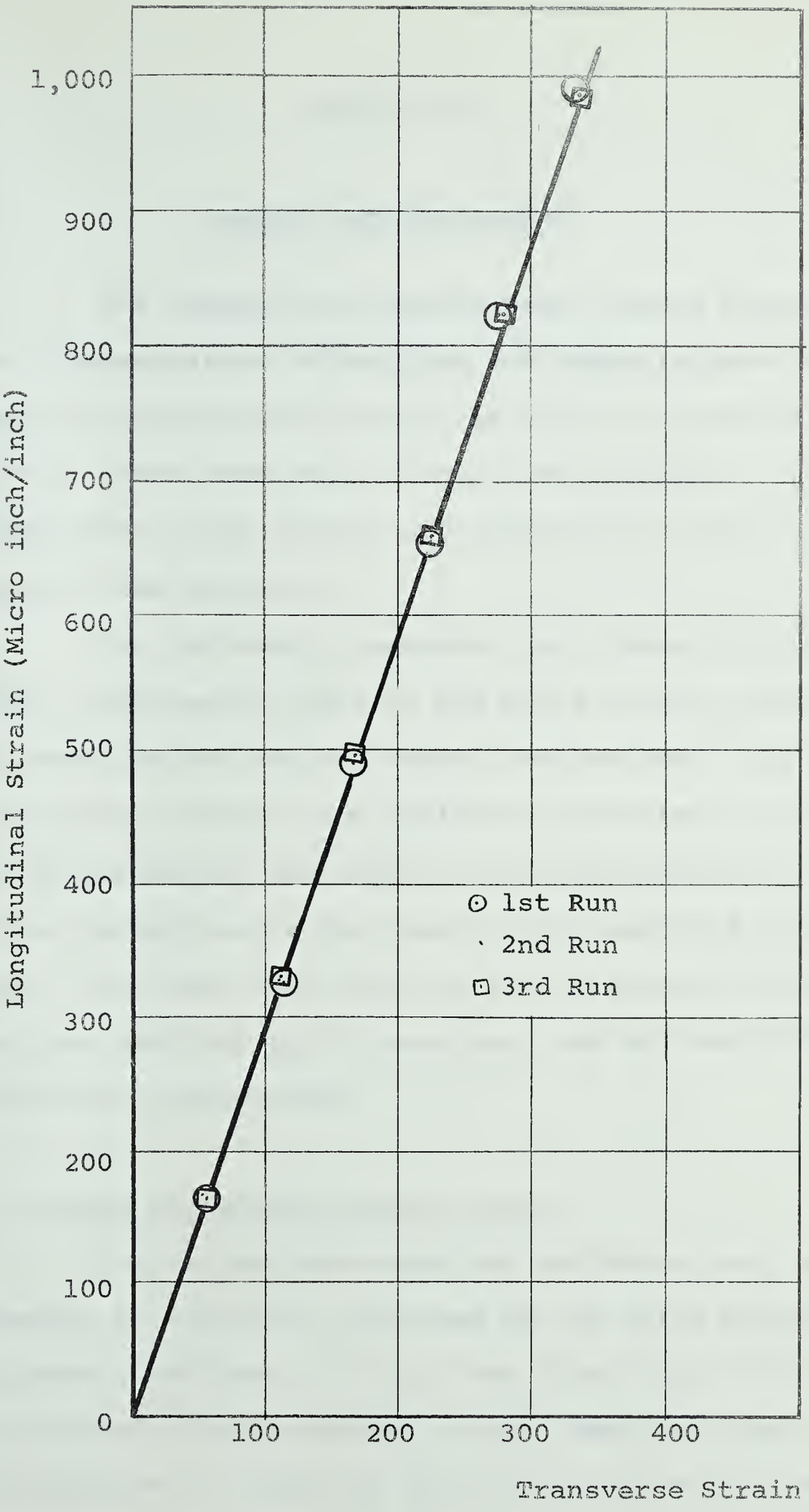

Fig. 15. Longitudinal Strain versus Transverse Strain for Tensile Test on Brass.

CHAPTER IV

RESULTS AND DISCUSSION

The temperature distributions, Moiré fringe patterns, dimensionless deflections and dimensionless bending moments are presented in Figs. 16 to 37, for the three kinds of tests conducted in this investigation. The temperature data, experimental and theoretical results are tabulated in the appendix.

For the simply supported and clamped circular plates, experimental results and Moiré fringe patterns are presented for the horizontal and vertical grid directions. Moiré fringe patterns and deflection profiles are presented for the horizontal and vertical grid directions for the initial deflection of the elastically supported circular plate. Two tests were done for this case for the horizontal and vertical grid directions, and 45° and 135° grid directions, respectively.

4.1 Simply supported circular plate.

The deflections along the horizontal and vertical diameters of the plate, obtained by the Moiré method are very nearly the same. It is clear from Table A.3, that the theoretical deflections for the idealized case computed from equation (3) are only about one-tenth of the deflections

obtained by the Moiré method for the actual case. This disagreement among the deflections appears to be due to the following two reasons:-

1. The radial movement of the plate was partially constrained at the edge, therefore it deflected more than it would have, had it been free to move radially at the edge.
2. The deflection given by equation (3) does not take into account the radial temperature gradient.

From Fig. 19, it is seen that the radial bending moment, M_r is not zero at the edge of the plate. This indicates that true simple support boundary conditions were not achieved for this test. The dimensionless bending moments for the horizontal and vertical grid directions are in good agreement, except near the centre of the plate. This is due to the fact that it was difficult to trace the fringes near the centre of the plate, because of interference by the thermocouple wires. From Table A.4, the dimensionless bending moments for the idealized case computed from equations (5) are only a fraction of the dimensionless bending moments obtained by the Moiré method for the actual case. It is interesting to note that the theoretical dimensionless bending moments computed from equations (5) do not agree in sign with the dimensionless bending moments obtained by the Moiré method. This is explained by the fact that the temperature

term in equations (5) is comparatively large, and while computing the moments by the Moiré method the curvature terms are of a higher order of magnitude.

4.2 Clamped circular plate.

In this test the Moiré fringe patterns for the horizontal and vertical grid directions were not exactly similar. It is to be noted that the same infrared heat lamp was used to heat the clamped circular plates as was used to heat the simply supported circular plates. The boundary conditions for the simply supported and clamped circular plates were quite uniform. Therefore, it appears that this lack of similarity between the two Moiré fringe patterns could be caused by the initial curvatures in the plate, introduced by the spot welding of thermocouples.

It is seen from Fig. 23 that the plate deflected more along the horizontal diameter (i.e. for vertical grid direction). This could be explained by the fact that the plate warped more along the horizontal diameter, due to the spot welding of the thermocouples. It is seen from Table A.7 that the theoretical deflections for the idealized case given by equation (3) are very small in comparison with the deflections obtained by the Moiré method for the actual case. This disagreement among the deflections appears to be due to the same reasons as for the simply supported case.

The curves for dimensionless bending moments are symmetrical about the centre of the plate for each grid direction. The bending moments M_r and M_θ are larger at the edge for the vertical grid direction than the bending moments at the edge for the horizontal grid direction. This is supported by the Moiré fringe patterns, since the fringes are closer near the edge for vertical grid direction as compared with the fringes near the edge for the horizontal grid direction. The value of the dimensionless bending moments for the horizontal grid direction at the centre of the plate given by Moiré method is 53.974. The plotting of the curves show that this point is in error. This is due to the error in analysis, because the fringes were very close together and hidden by the thermocouple wires near the centre of the plate for the horizontal grid direction, and so it was difficult to locate them exactly.

From Table A.8 the theoretical dimensionless bending moments for an idealized case computed from equations (5) are very small in comparison with the dimensionless bending moments obtained by the Moiré method for the actual case. The theoretical and Moiré method dimensionless bending moments do not agree in sign due to the same reasons as for the simply supported case.

4.3 Elastically supported circular plate.

It is seen from Fig. 27 that the initial deflection profiles for the horizontal and vertical grid directions are in good agreement.

It was not possible to compare the results of this test, since there are no theoretical solutions available for this case. The boundary of this plate is neither simply supported nor clamped. It is observed from the Moiré fringe patterns of this test that the boundary conditions are close to those of a clamped boundary.

From Figs. 31 and 35, the dimensionless deflections along the two respective perpendicular diameters are in good agreement, except near the centre of the plate. It is noted that the fringes are close together and hidden under the thermocouple wires near the centre of the plate, and are difficult to locate.

The dimensionless bending moment curves for each grid direction are symmetrical about the centre of the plate, and are in good agreement for the respective perpendicular grid directions except near the edge of the plate. The bending moments tend to be constant within a radius of one inch from the centre of the plate. It is noted that the Moiré fringes in this region are almost straight and equally spaced.

In these tests for horizontal and vertical grid directions, and for 45° and 135° grid directions the average maximum deflections due to thermal loading were 0.03768 in. and 0.03126 in. respectively.

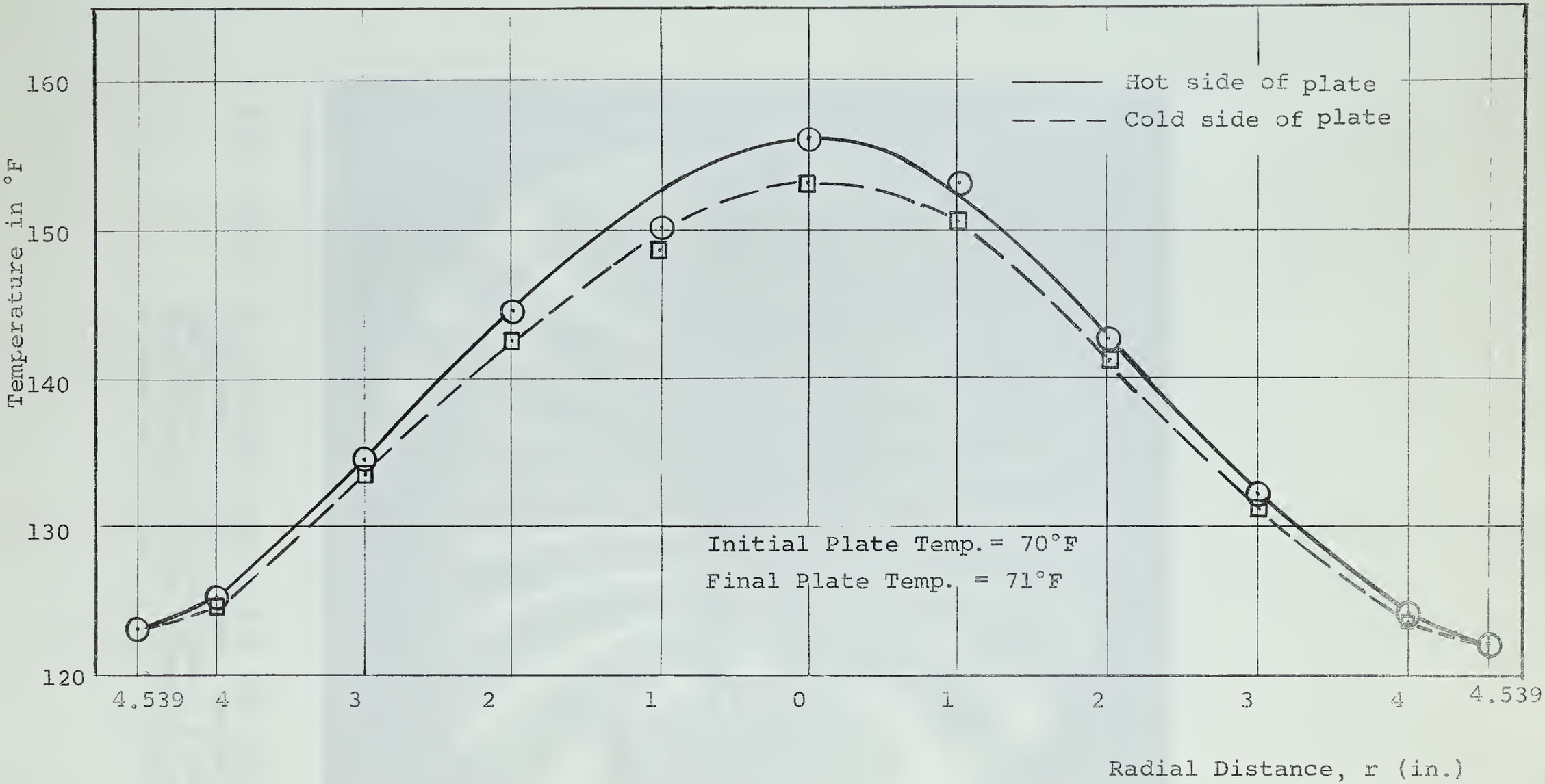

Fig. 16. Temperature Distribution for the Simply Supported Circular Plate.

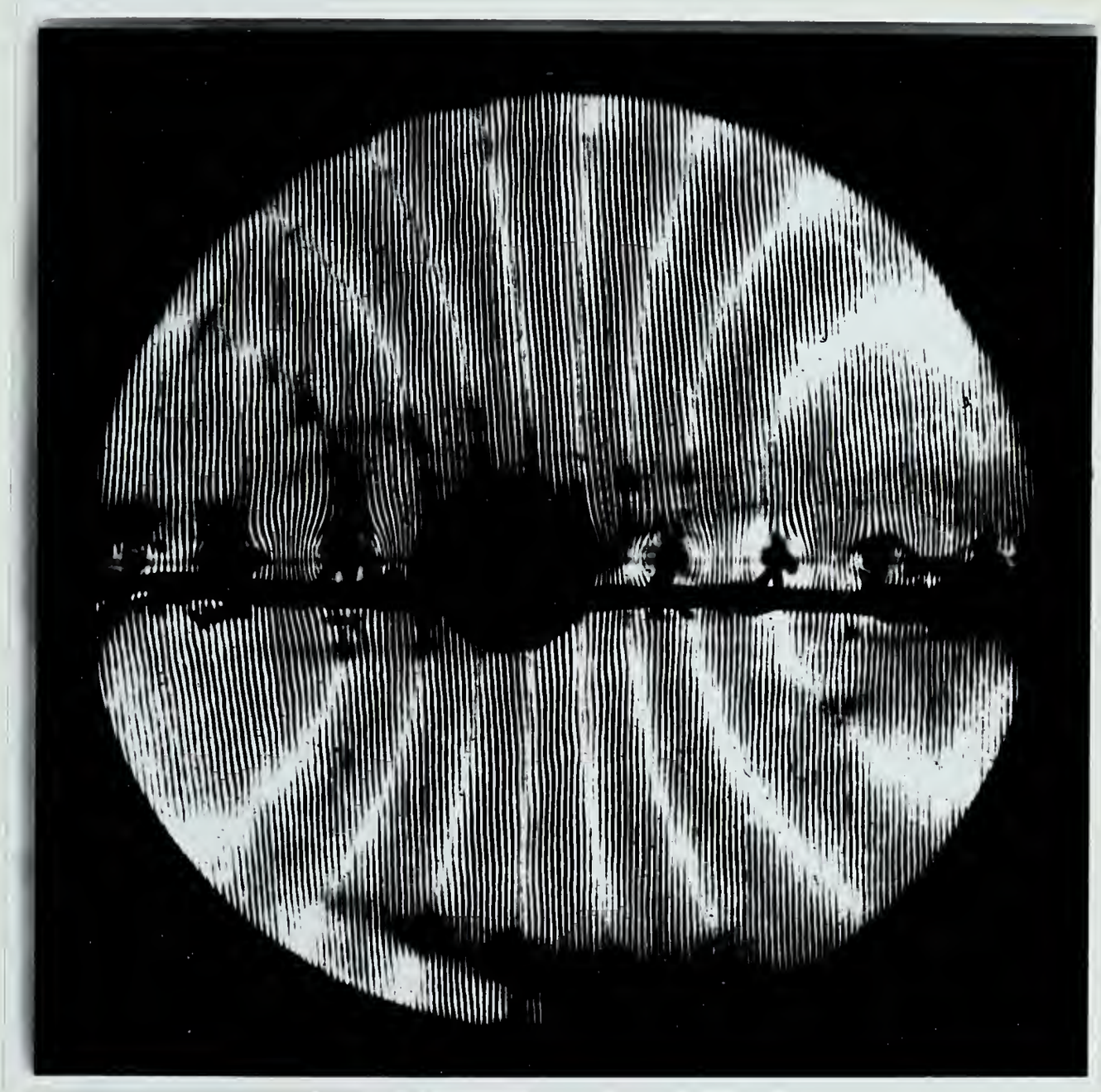

Fig. 17(a). Moiré Fringe Pattern for the Simply Supported Circular Plate, heated at the centre. Grid Vertical. 0.063 in. thick aluminum plate, diameter = 9.078 in. Maximum Deflection, w_{max} = 0.02755 in.

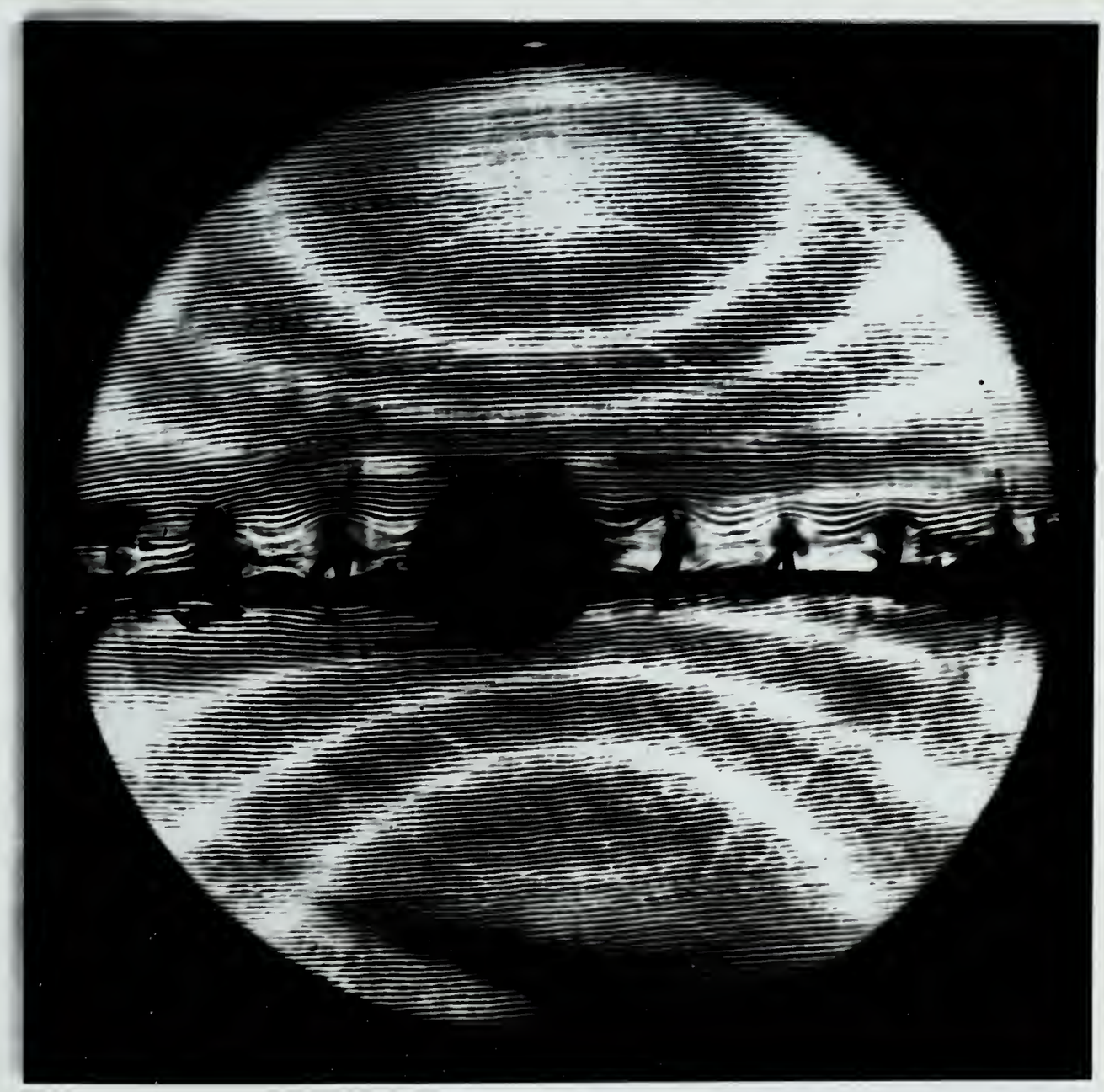

Fig. 17(b). Moiré Fringe Pattern for the Simply Supported Circular Plate, heated at the centre. Grid horizontal. 0.063 in. thick aluminum plate, diameter = 9.078 in. Maximum Deflection, w_{max} = 0.02787 in.

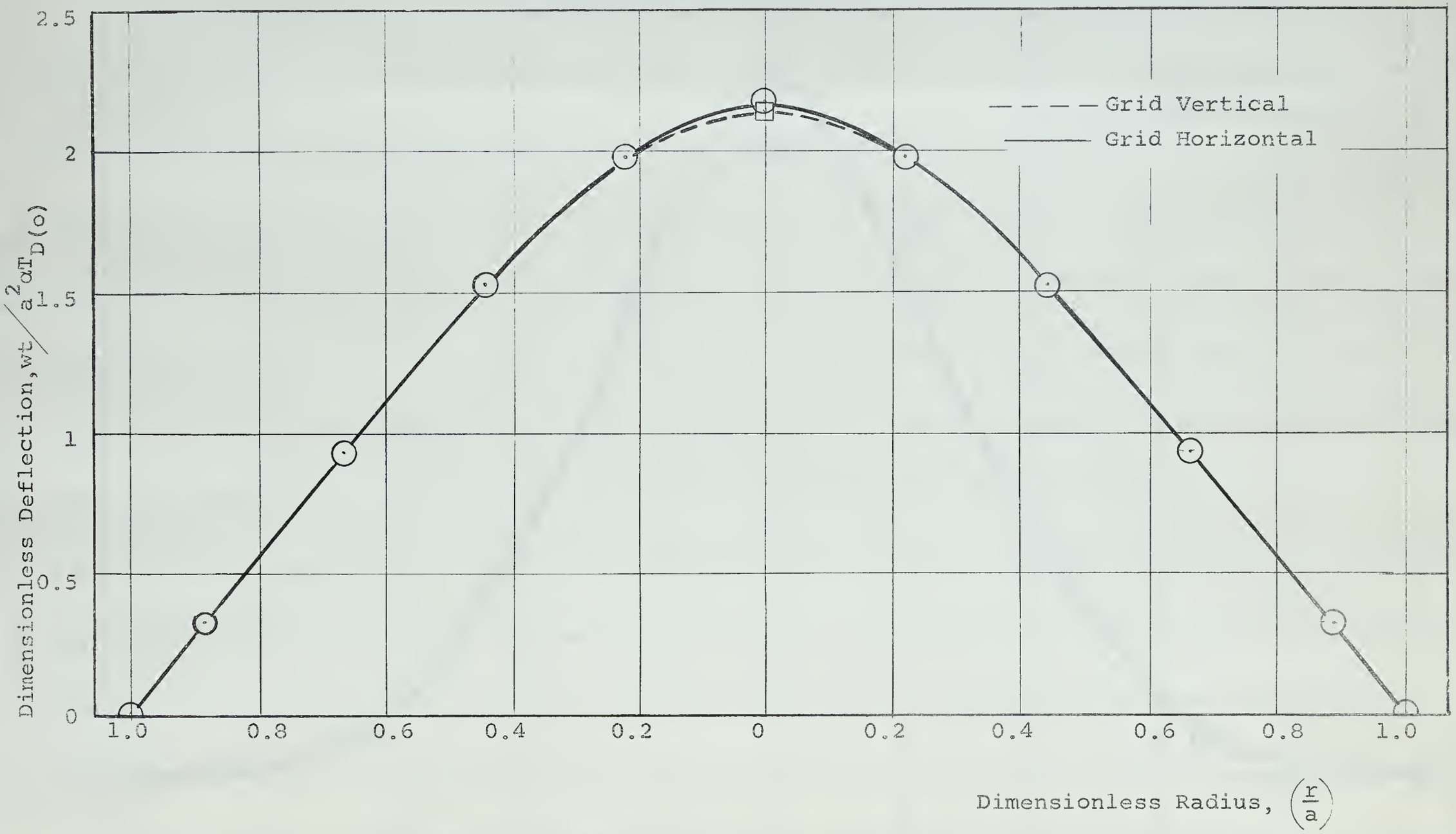

Fig. 18. Dimensionless Deflection, $wt/a^2\alpha T_{D(o)}$ versus Dimensionless Radius, $\left(\frac{r}{a}\right)$ for the Simply Supported Circular Plate.

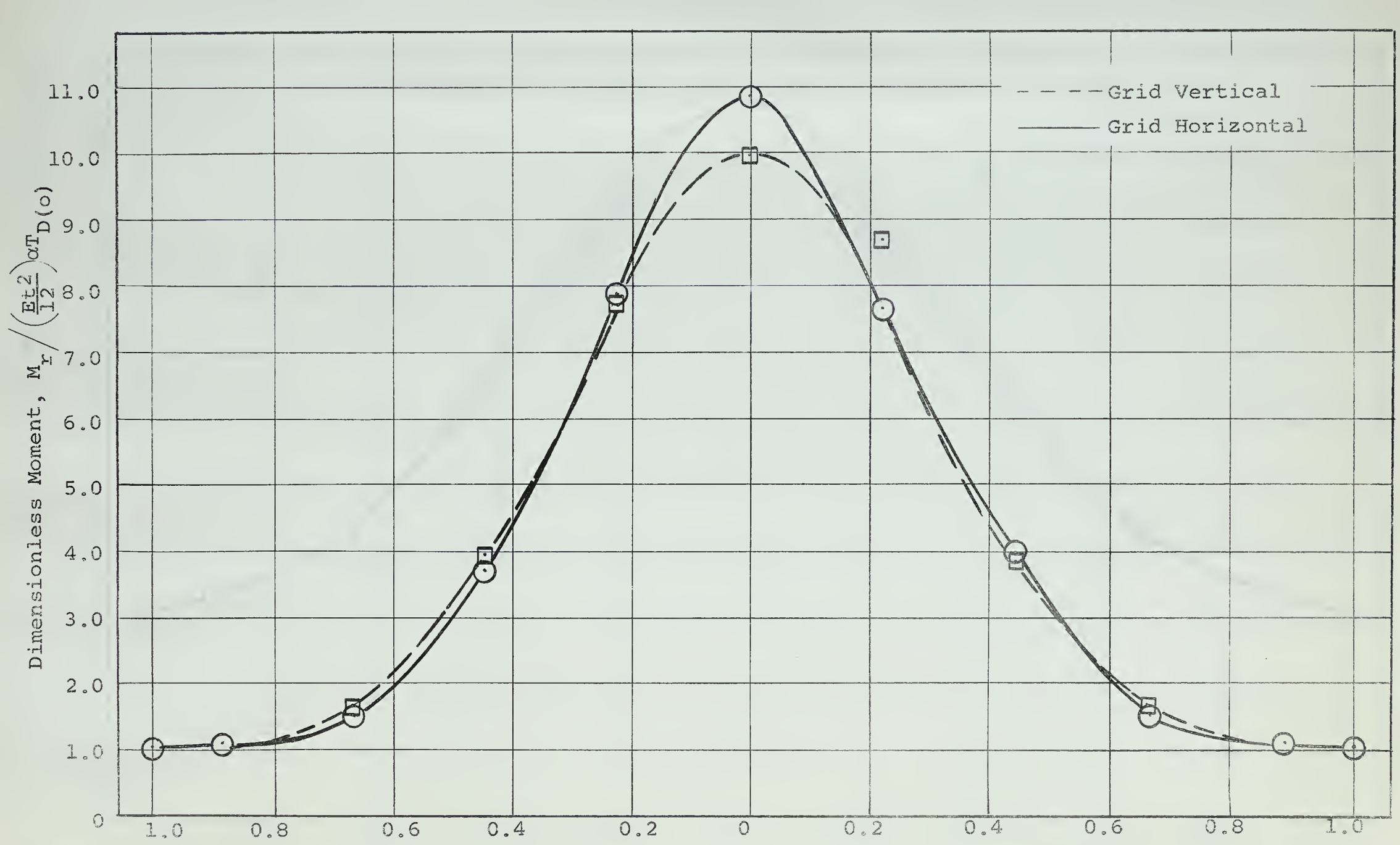

Fig. 19. Dimensionless Moment, $M_r \Big/ \left(\frac{Et^2}{12}\right)\alpha T_{D(o)}$ versus Dimensionless Radius, $\left(\frac{r}{a}\right)$ for the Simply Supported Circular Plate.

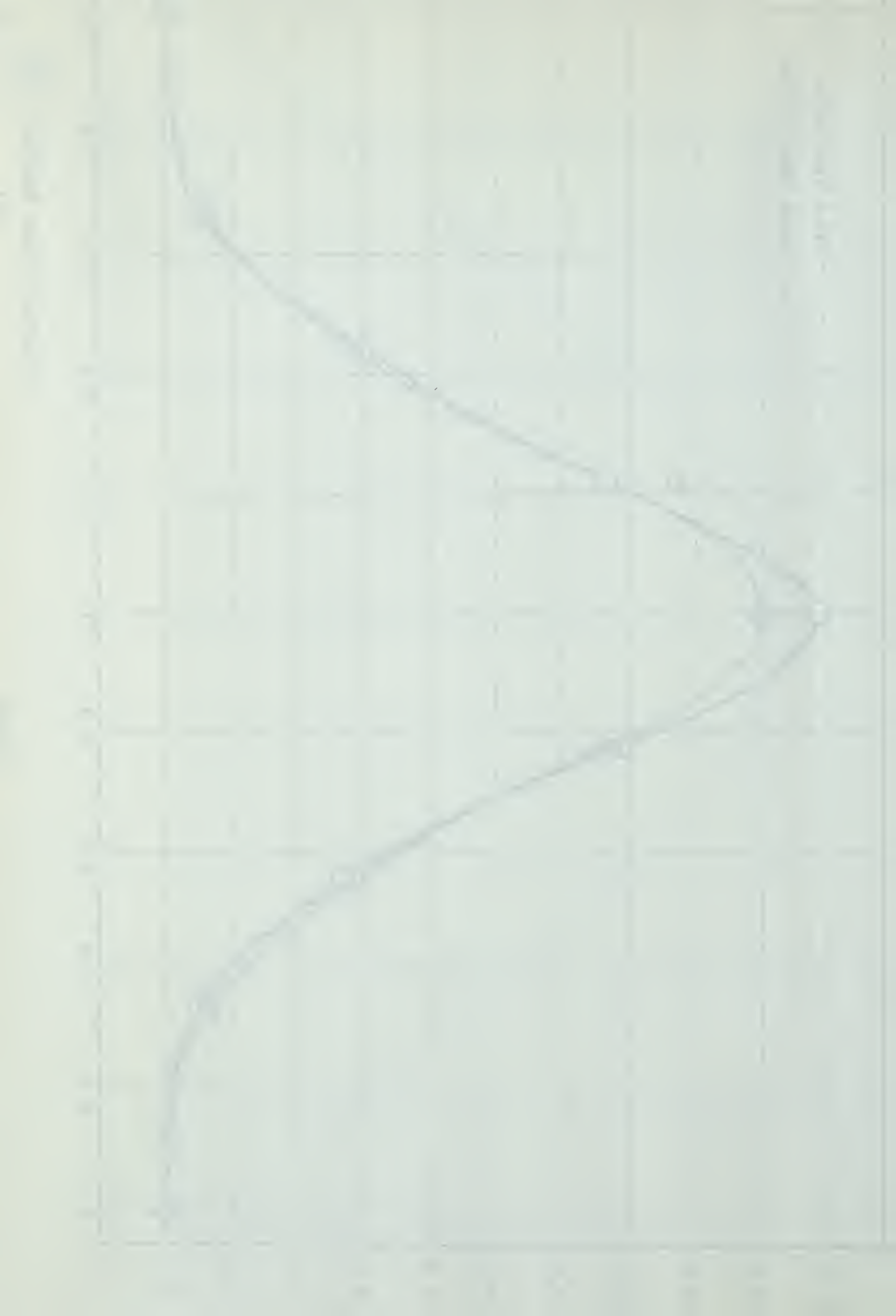

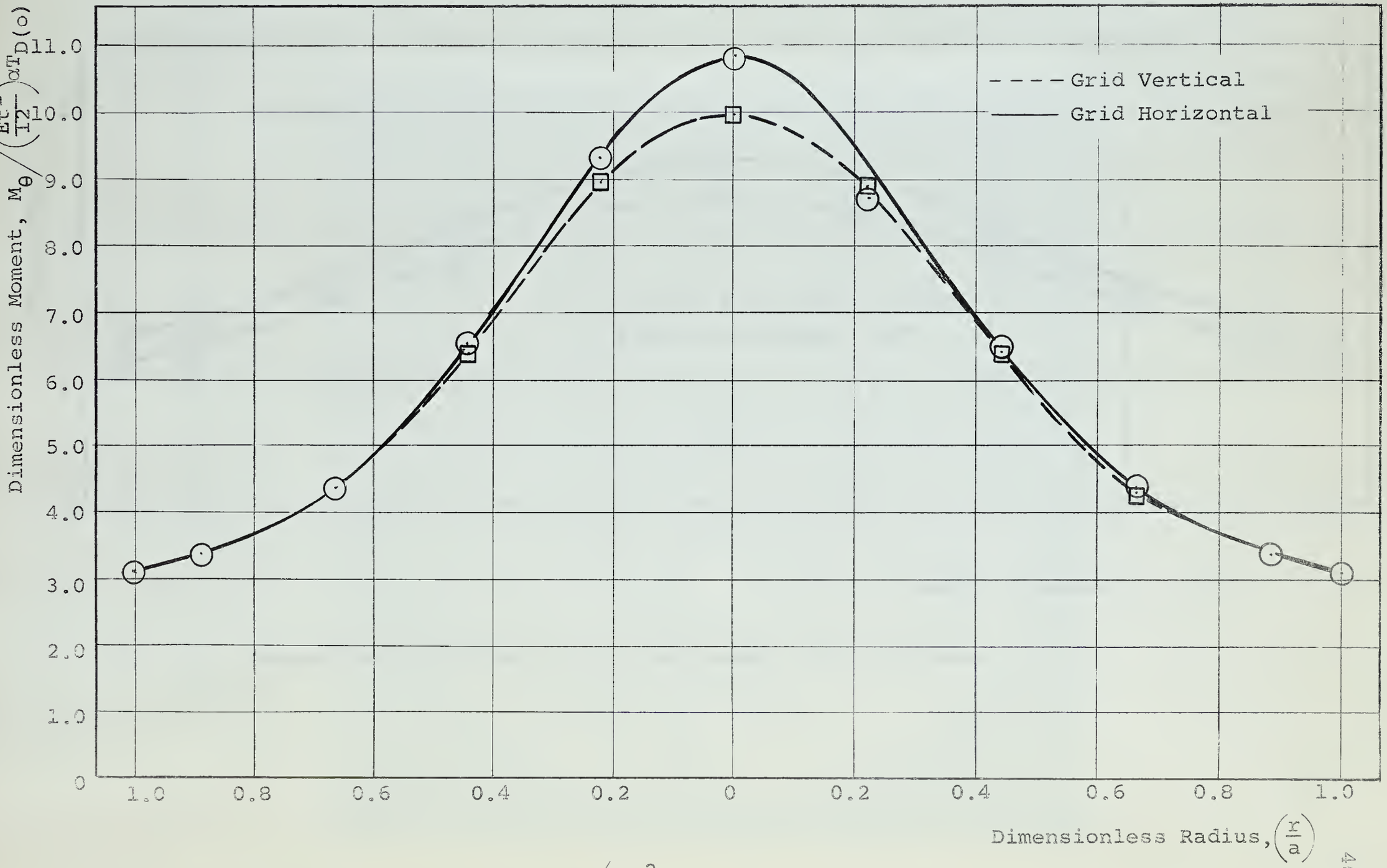

Fig. 20. Dimensionless Moment, $M_\theta \Big/ \left(\frac{Et^2}{12}\right)\alpha T_{D(o)}$ versus Dimensionless Radius, $\left(\frac{r}{a}\right)$ for the Simply Supported Circular Plate.

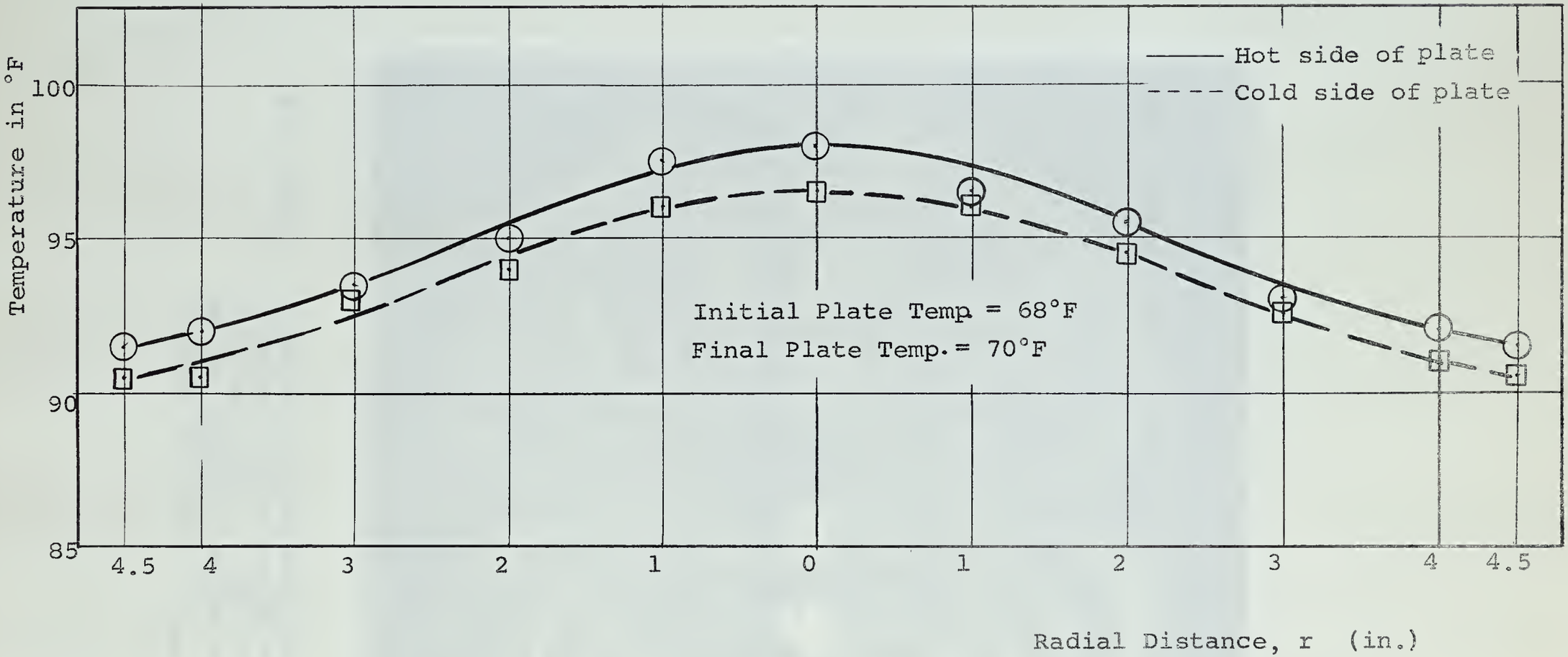

Fig. 21. Temperature Distribution for the Clamped Circular Plate.

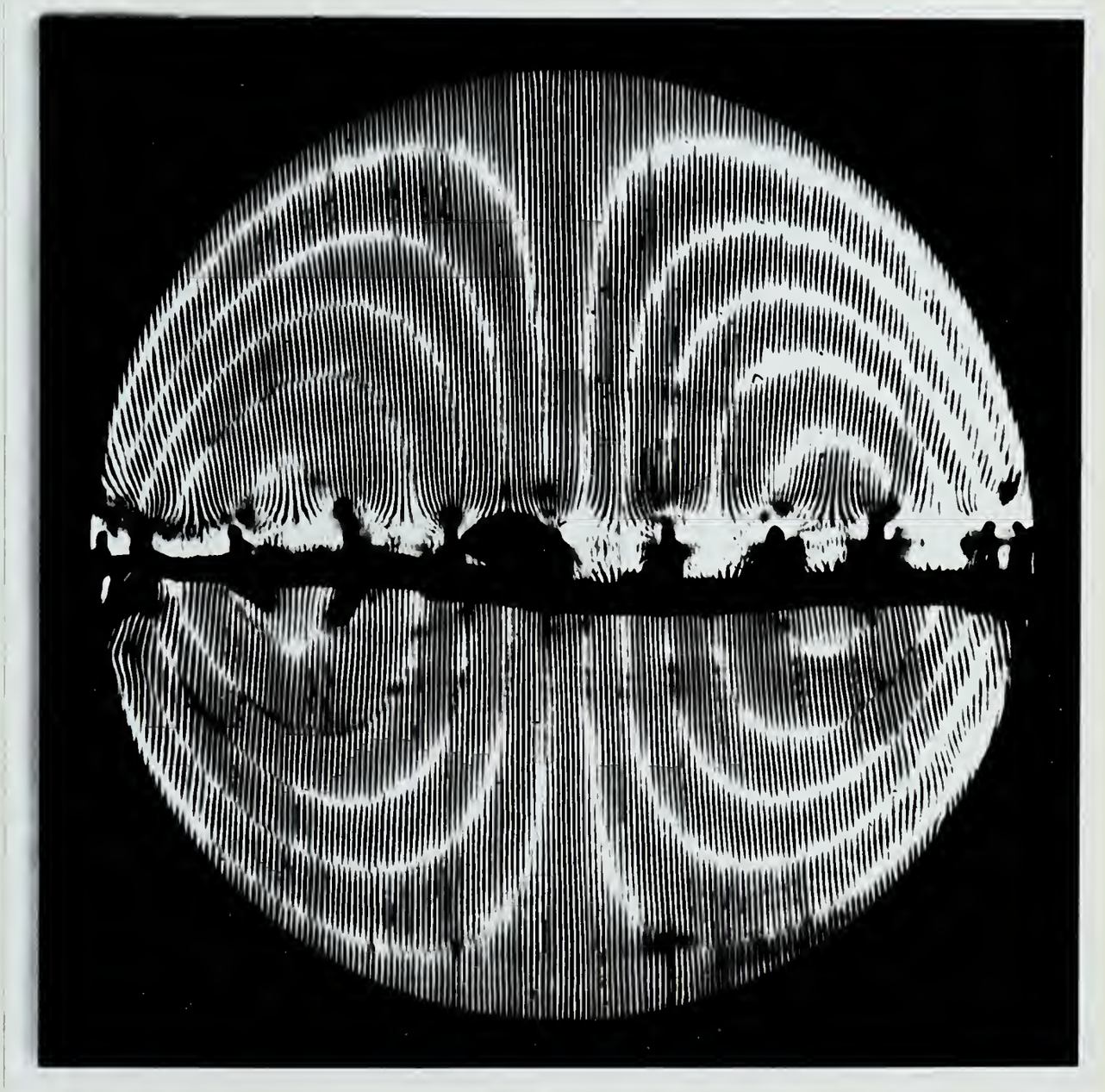

Fig. 22(a). Moiré Fringe Pattern for the Clamped Circular Plate, heated at the centre. Grid vertical. 0.063 in. thick aluminum plate, diameter = 9.0 in. Maximum Deflection, w_{max} = 0.02982 in.

Fig. 22(b). Moiré Fringe Pattern for the Clamped Circular Plate, heated at the centre. Grid horizontal. 0.063 in. thick aluminum plate, diameter = 9.0 in. Maximum Deflection, w_{max} = 0.02800 in.

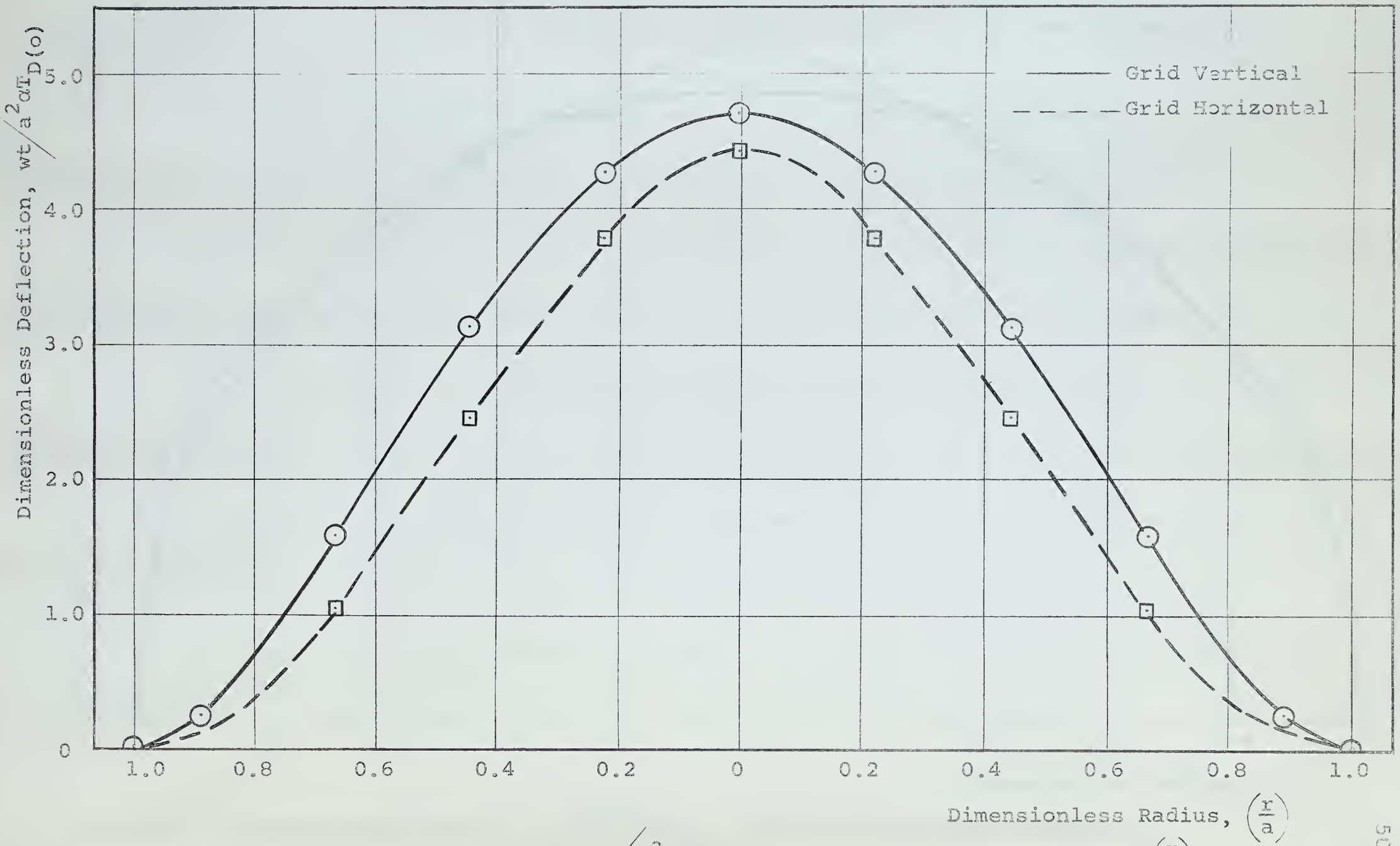

Fig. 23. Dimensionless Deflection, $wt/a^2\alpha T_{D(o)}$ versus Dimensionless Radius, $\left(\frac{r}{a}\right)$ for the Clamped Circular Plate.

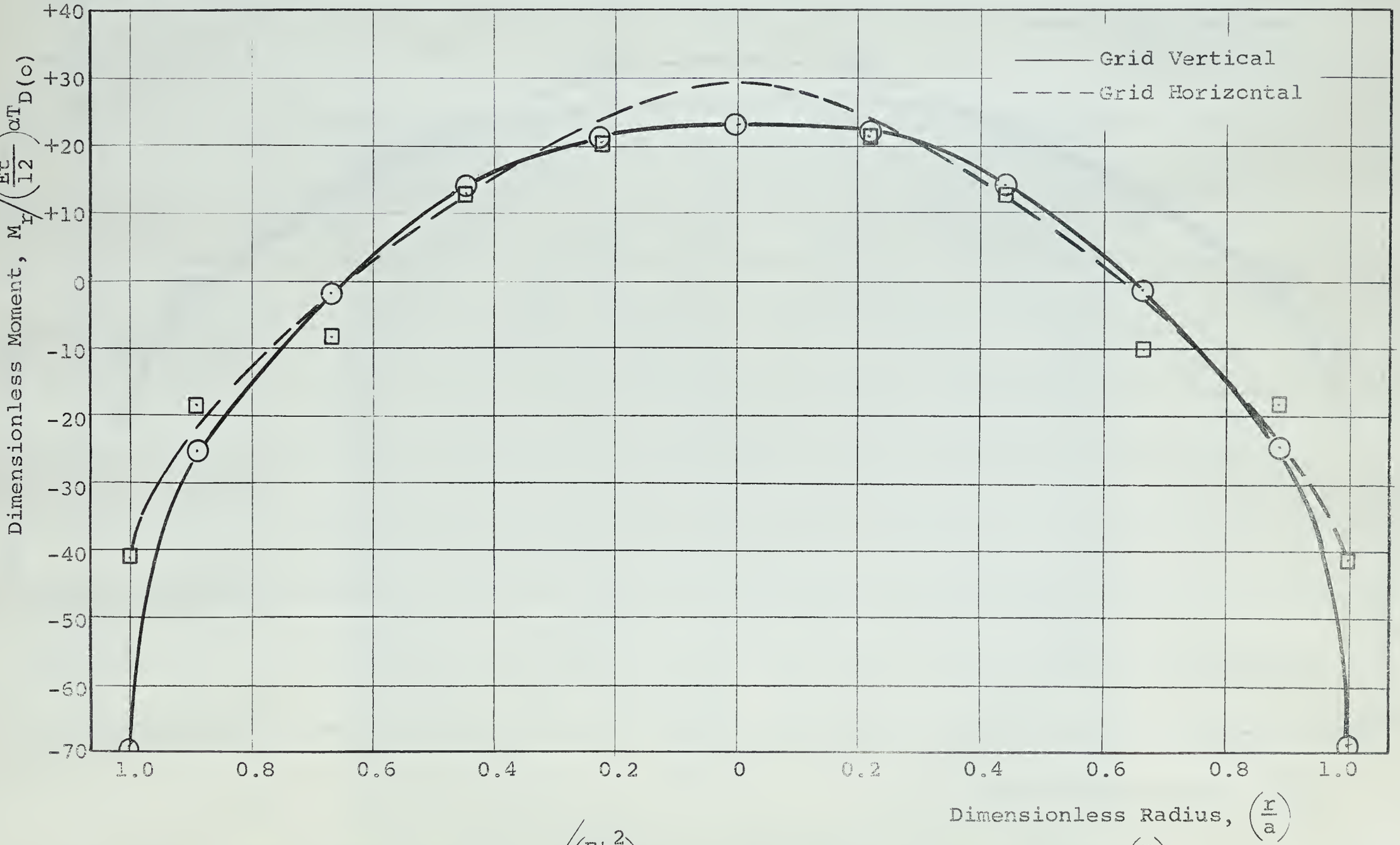

Fig. 24. Dimensionless Moment, $M_r \Big/ \left(\frac{Et^2}{12}\right)\alpha T_{D(o)}$ versus Dimensionless Radius, $\left(\frac{r}{a}\right)$ for the Clamped Circular Plate.

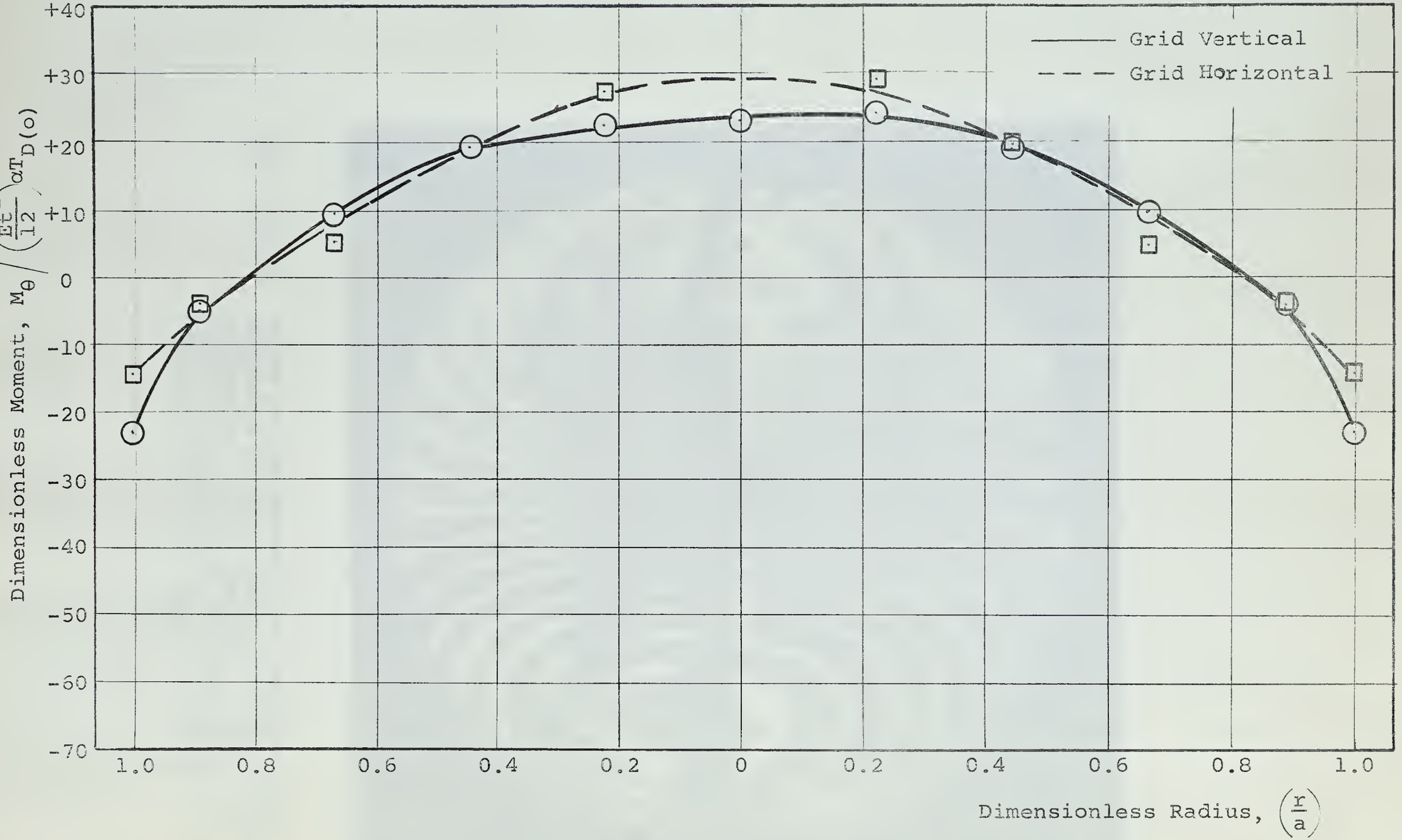

Fig. 25. Dimensionless Moment, $M_\theta \Big/ \left(\frac{Et^2}{12}\right)\alpha T_{D(o)}$ versus Dimensionless Radius, $\left(\frac{r}{a}\right)$ for the Clamped Circular Plate.

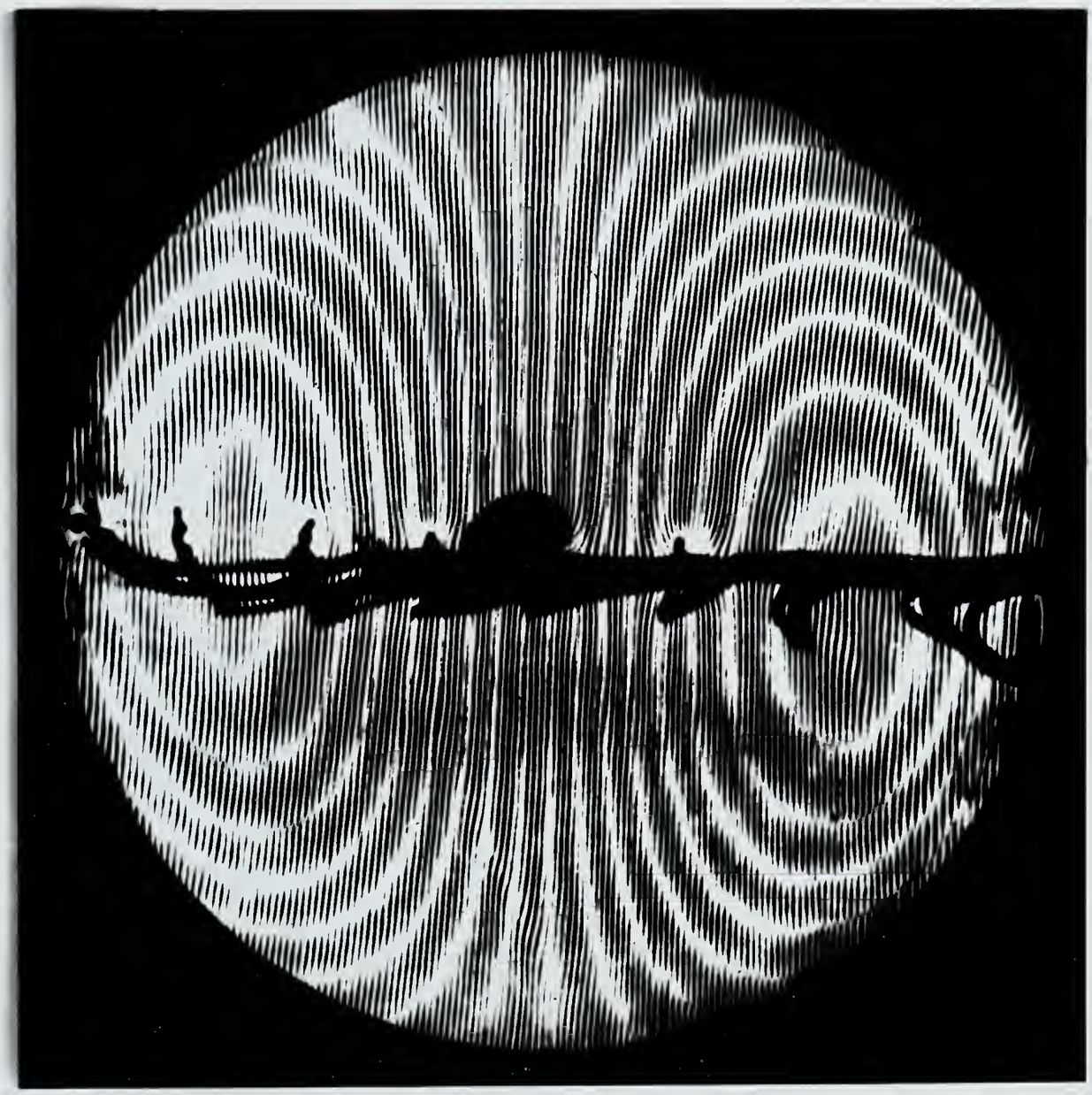

Fig. 26(a). Moiré Fringe Pattern for the Elastically Supported Circular Plate, for the Initial Deflection. Grid vertical. 0.063 in. thick aluminum plate, diameter = 8.016 in. Maximum Deflection, w_{max} = 0.04508 in.

Fig. 26(b). Moiré Fringe Pattern for Elastically Supported Circular Plate, for the Initial Deflection. Grid Horizontal. 0.063 in. aluminum plate, diameter = 8.016 in. Maximum Deflection, w_{max} = 0.04428 in.

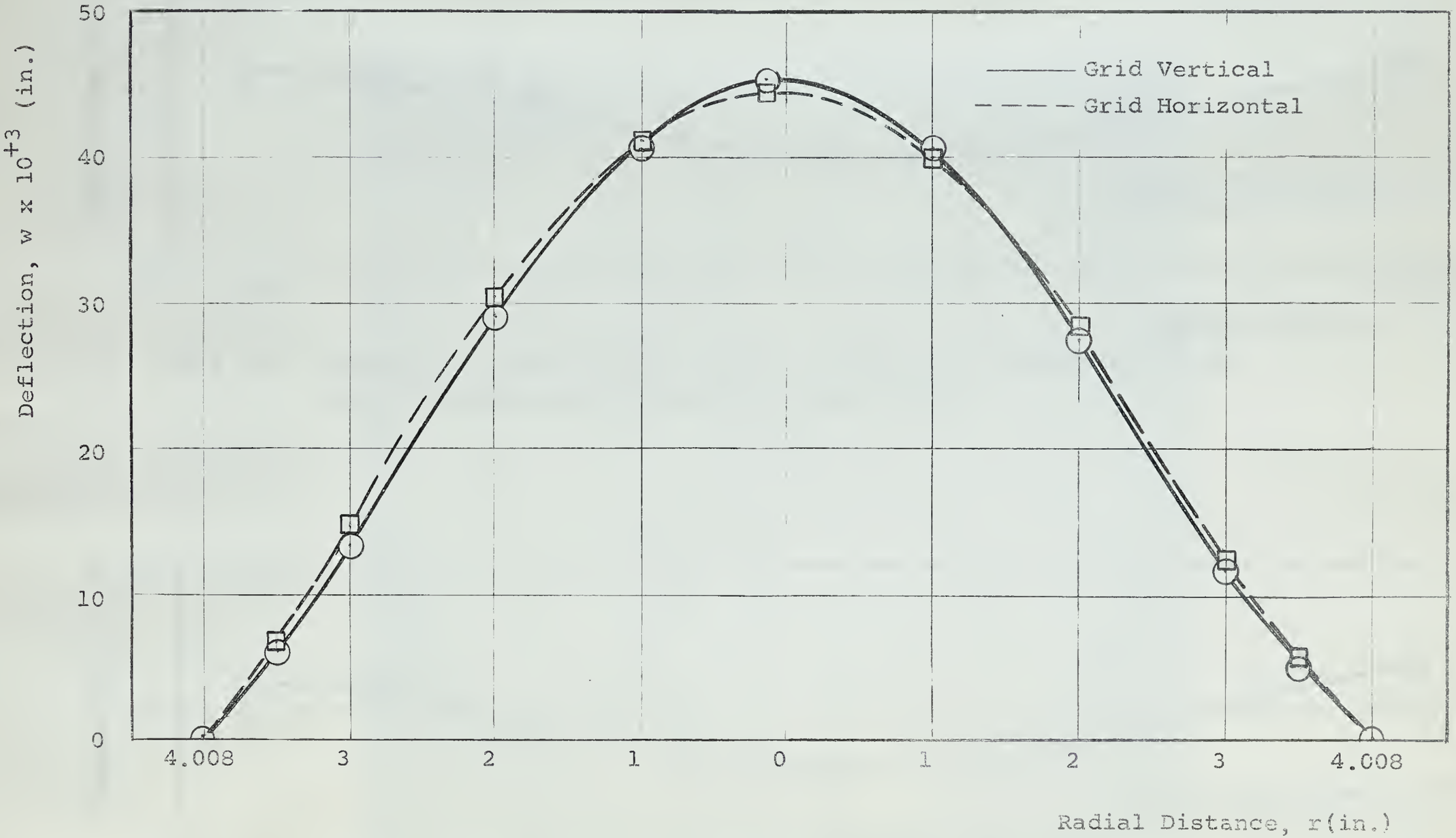

Fig. 27. Initial Deflection, w, versus Radius, r, for the Elastically Supported Circular Plate.

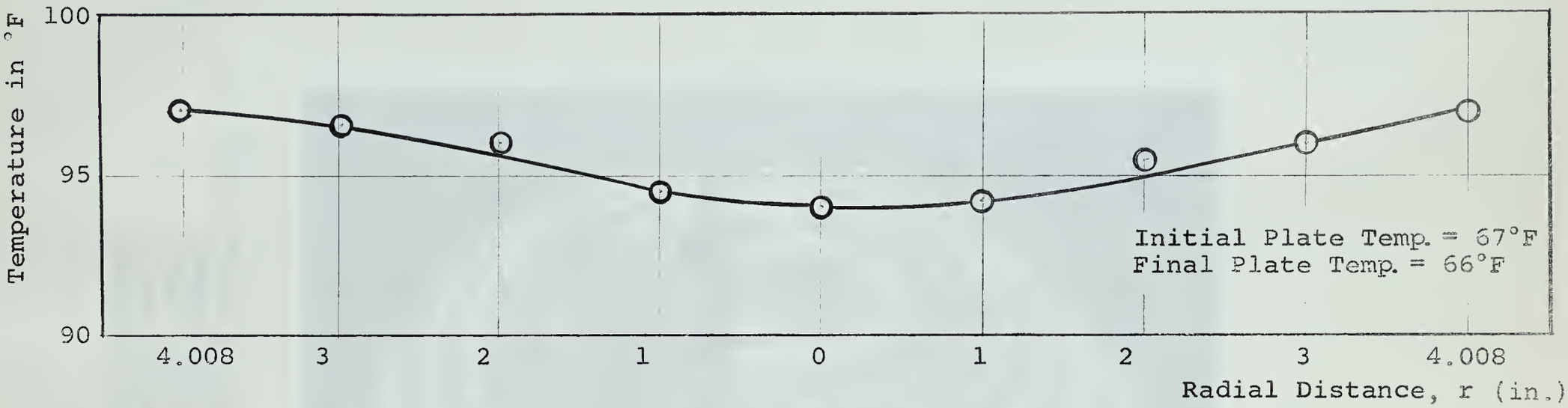

Fig. 29. Temperature Distribution for 45° and 135° Grid Directions Test, for the Elastically Supported Circular Plate.

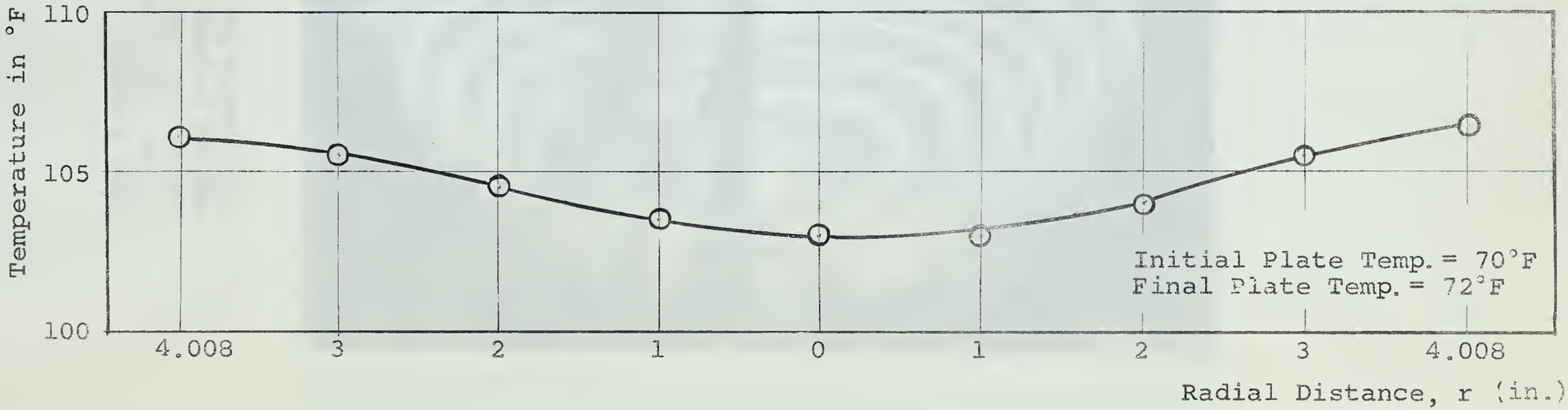

Fig. 28. Temperature Distribution for 0° and 90° Grid Directions Test, for the Elastically Supported Circular Plate.

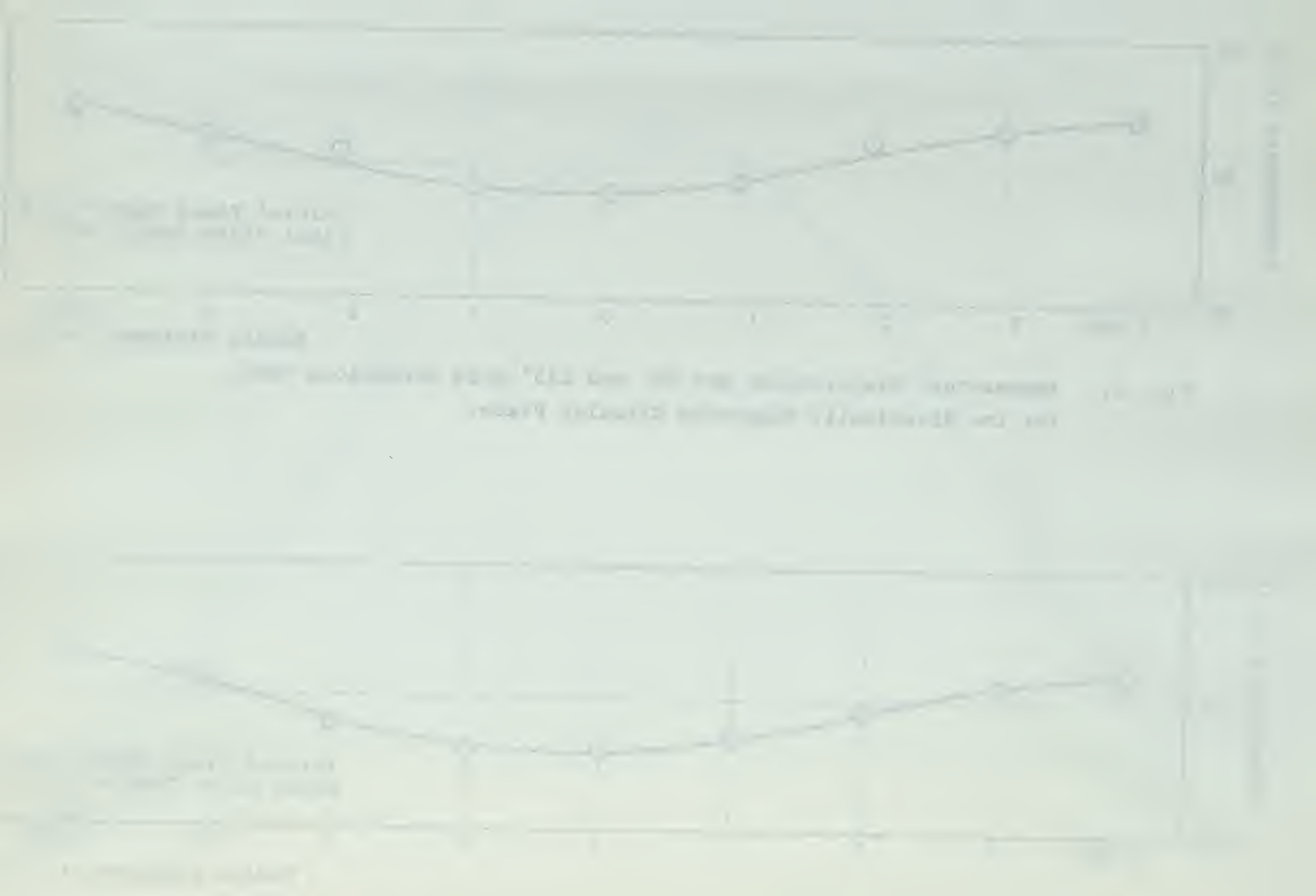

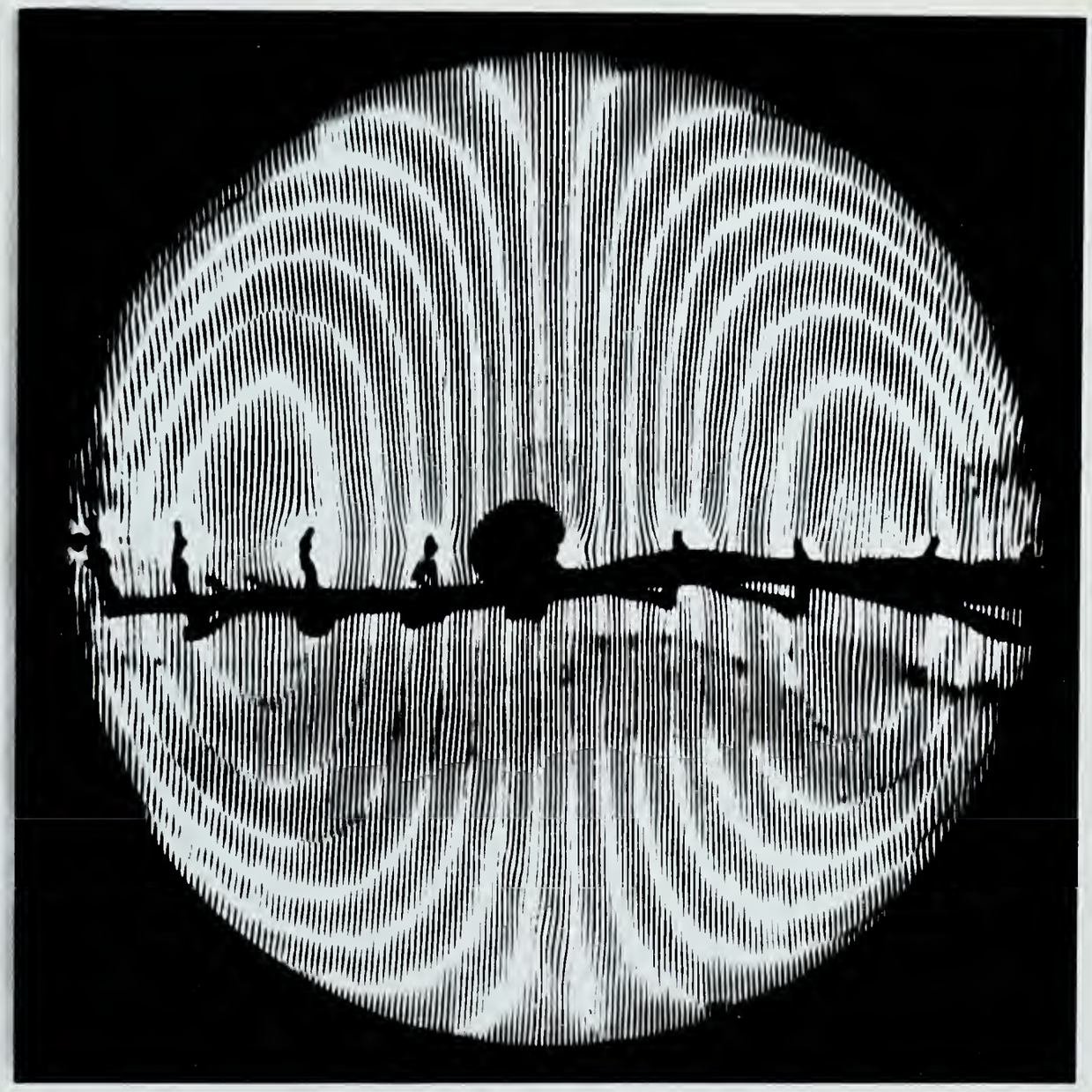

Fig. 30(a). Moiré Fringe Pattern for the Elastically Supported Circular Plate, heated at the edge. Grid Vertical. 0.063 in. thick aluminum plate, diameter = 8.016 in. Maximum Deflection, w_{max} = 0.03913 in.

Fig. 30(b). Moiré Fringe Pattern for the Elastically Supported Circular Plate, heated at the edge. Grid Horizontal. 0.063 in. thick aluminum plate, diameter = 8.016 in. Maximum Deflection, w_{max} = 0.03622 in.

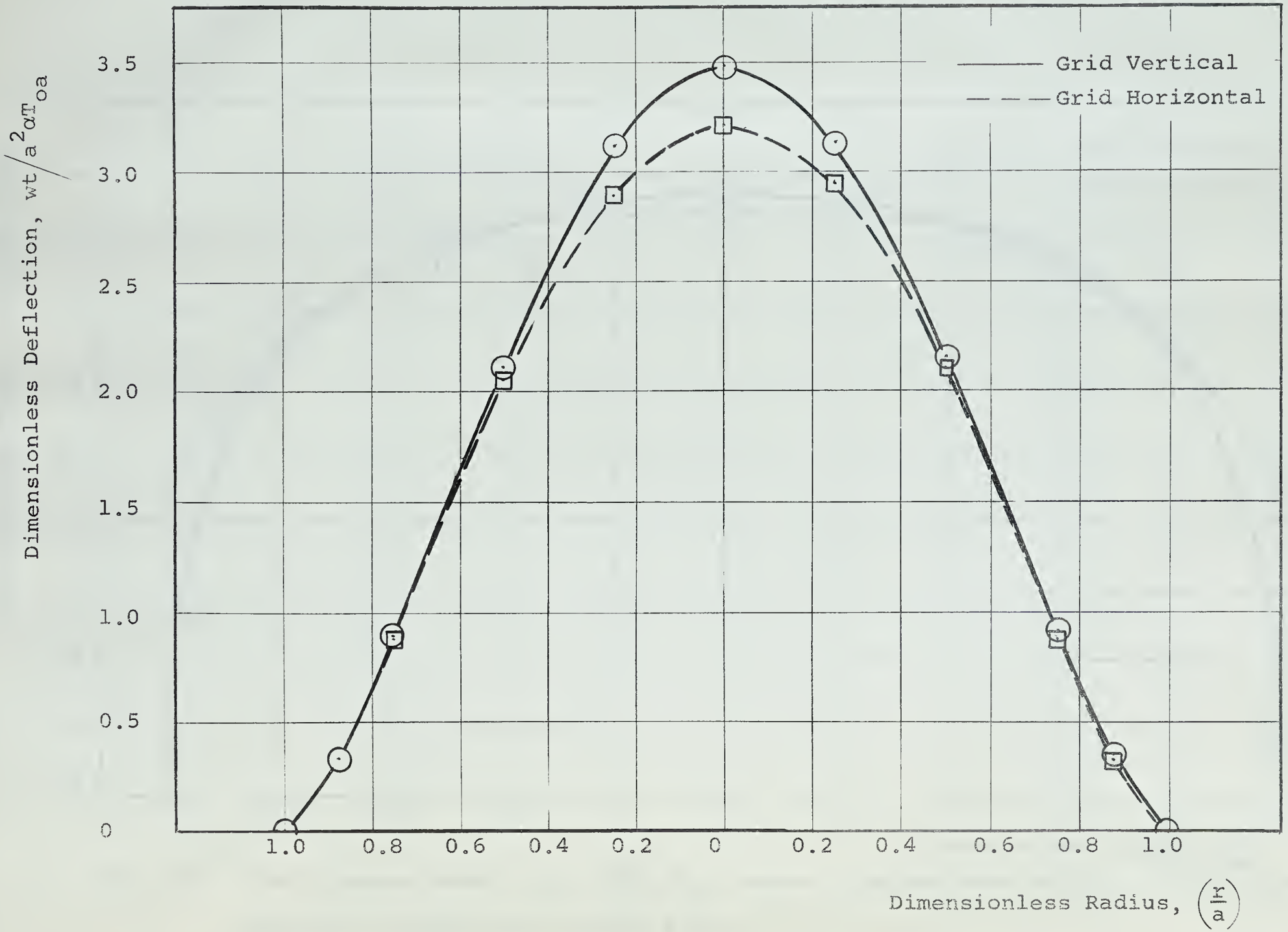

Fig. 31. Dimensionless Deflection, $Wt/a^2\alpha T_{oa}$ versus Dimensionless Radius, $\left(\frac{r}{a}\right)$ for the Elastically Supported Circular Plate.

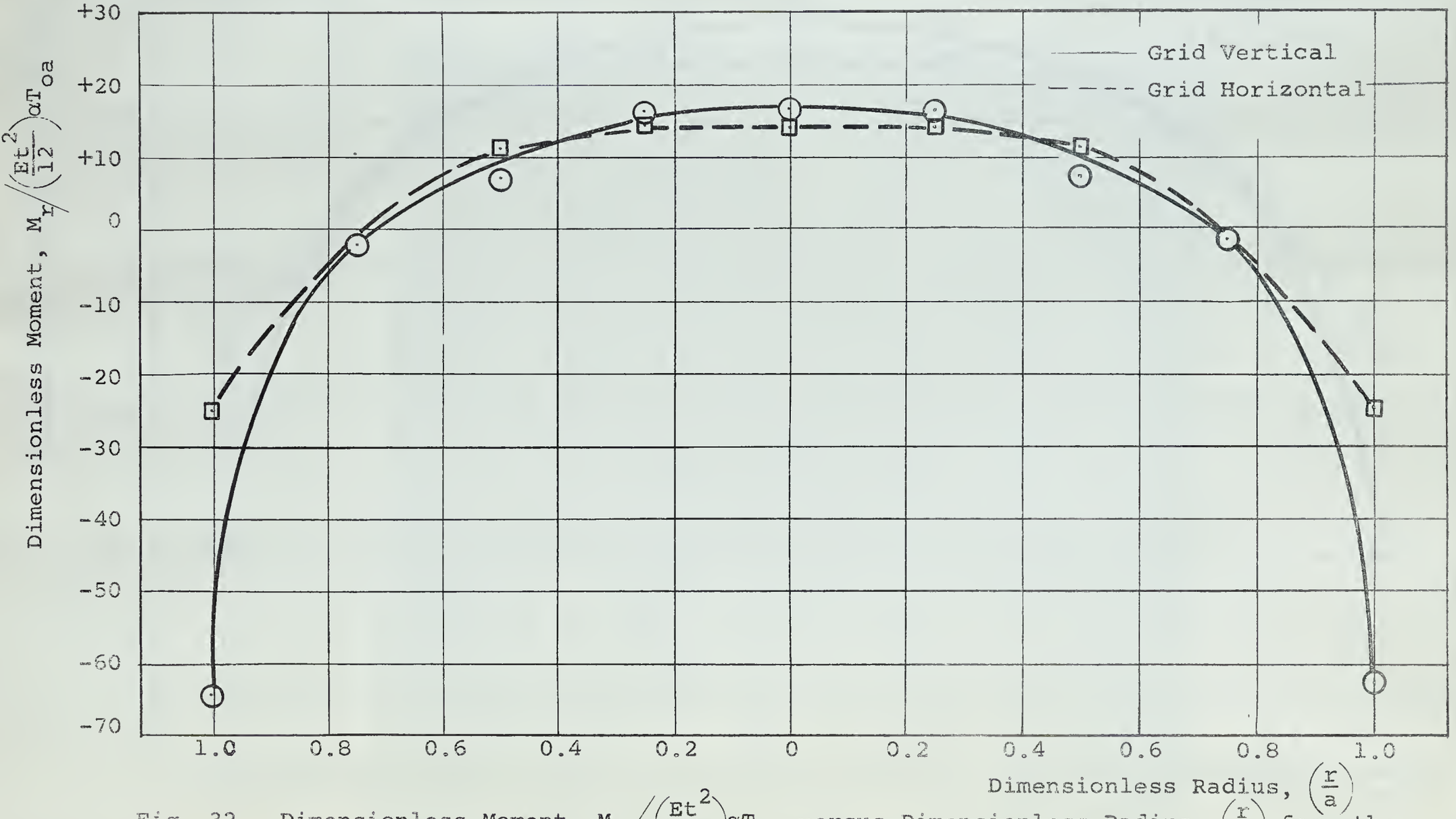

Fig. 32. Dimensionless Moment, $M_r/\left(\frac{Et^2}{12}\right)\alpha T_{oa}$ versus Dimensionless Radius, $\left(\frac{r}{a}\right)$ for the Elastically Supported Circular Plate.

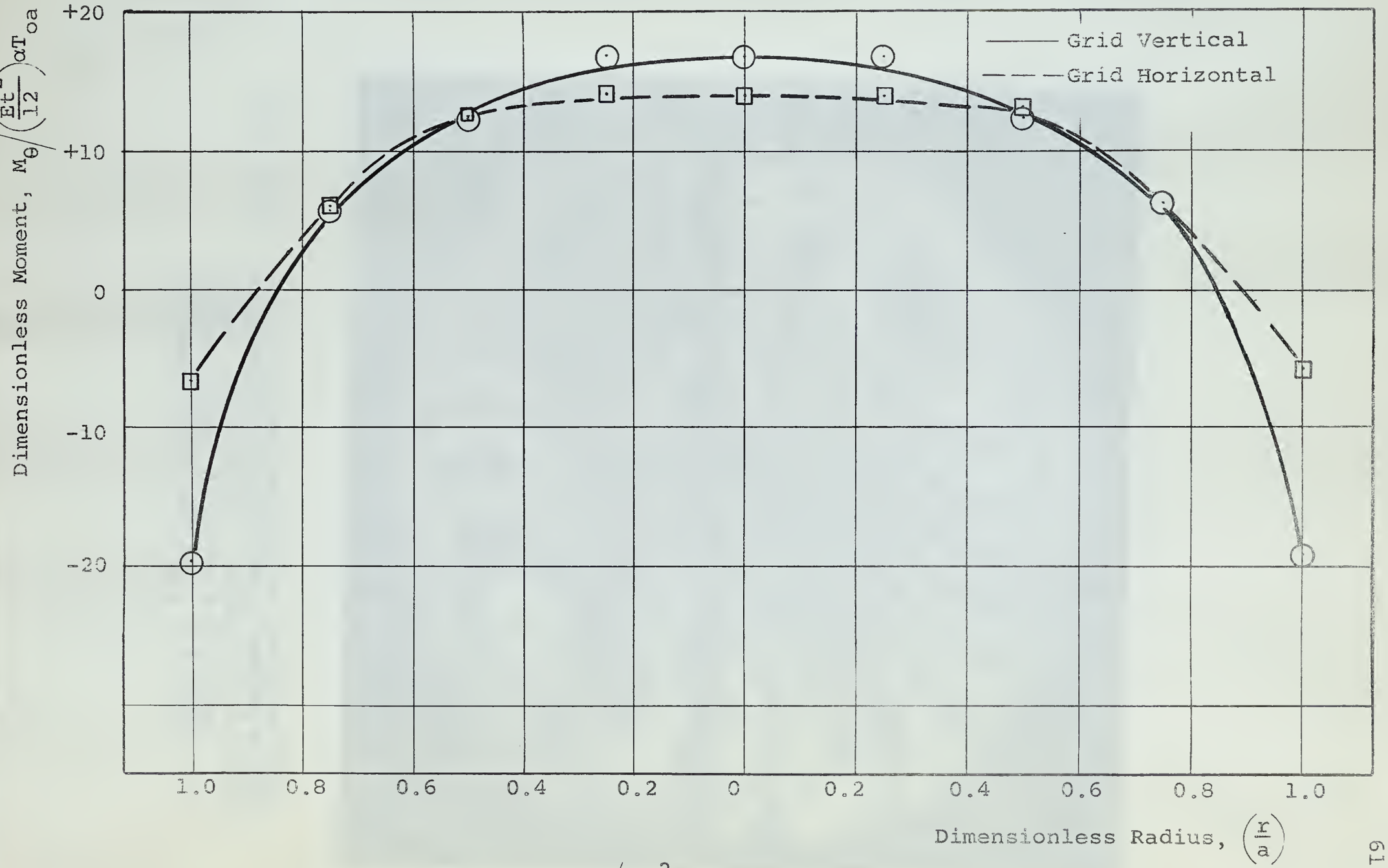

Fig. 33. Dimensionless Moment, $M_\theta \Big/ \left(\frac{Et^2}{12}\right)\alpha T_{oa}$ versus Dimensionless Radius, $\left(\frac{r}{a}\right)$ for the Elastically Supported Circular Plate.

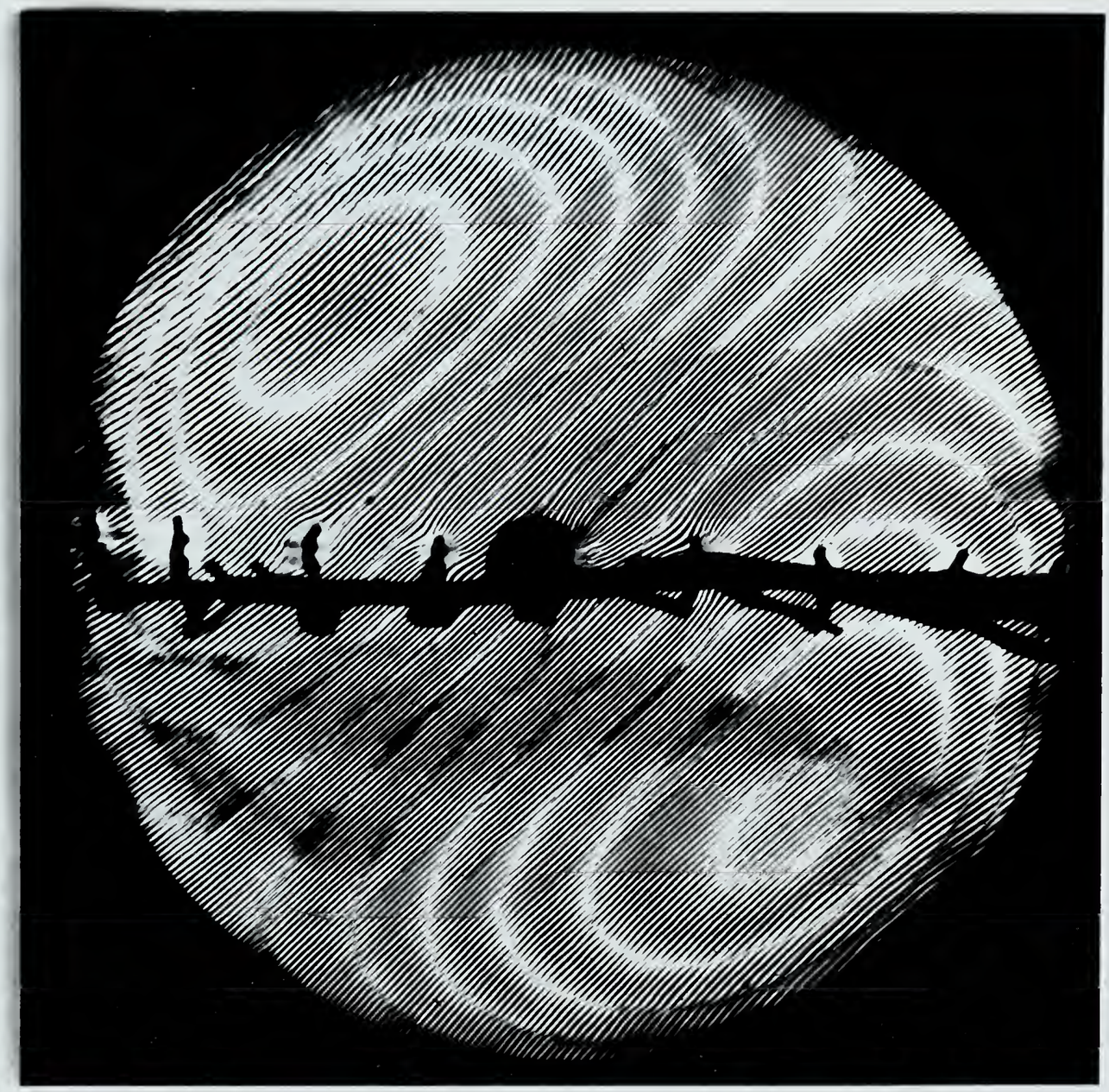

Fig. 34(a). Moiré Fringe Pattern for the Elastically Supported Circular Plate, heated at the edge. Grid at 45°. 0.063 in. thick aluminum plate, diameter = 8.016 in. Maximum Deflection, w_{max} = 0.03042 in.

Fig. 34(b). Moiré Fringe Pattern for the Elastically Supported Circular Plate, heated at the edge. Grid at 135°. 0.063 in. thick aluminum plate, diameter = 8.016 in. Maximum Deflection, w_{max} = 0.03210 in.

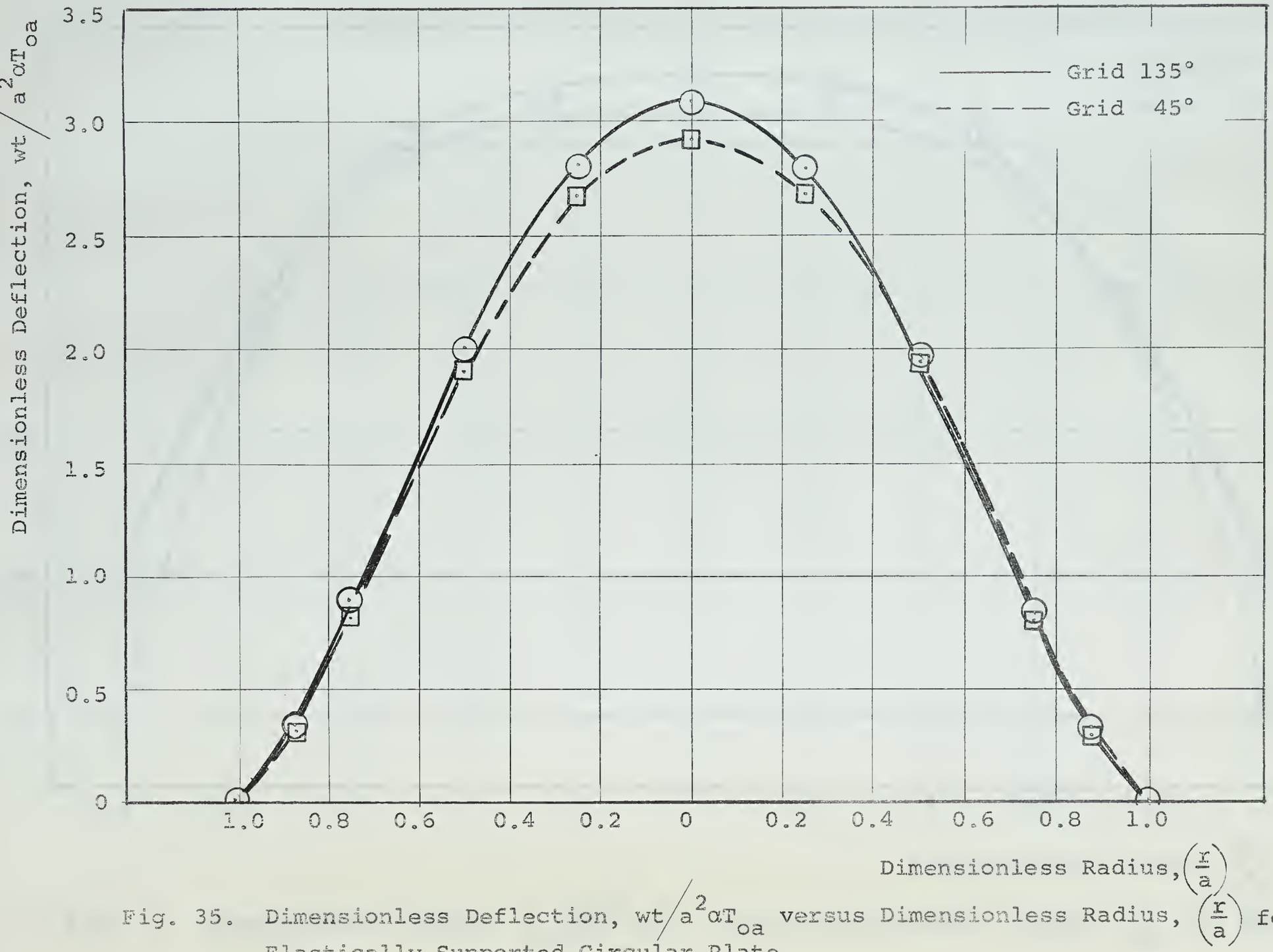

Fig. 35. Dimensionless Deflection, $wt/a^2\alpha T_{oa}$ versus Dimensionless Radius, $\left(\frac{r}{a}\right)$ for the Elastically Supported Circular Plate.

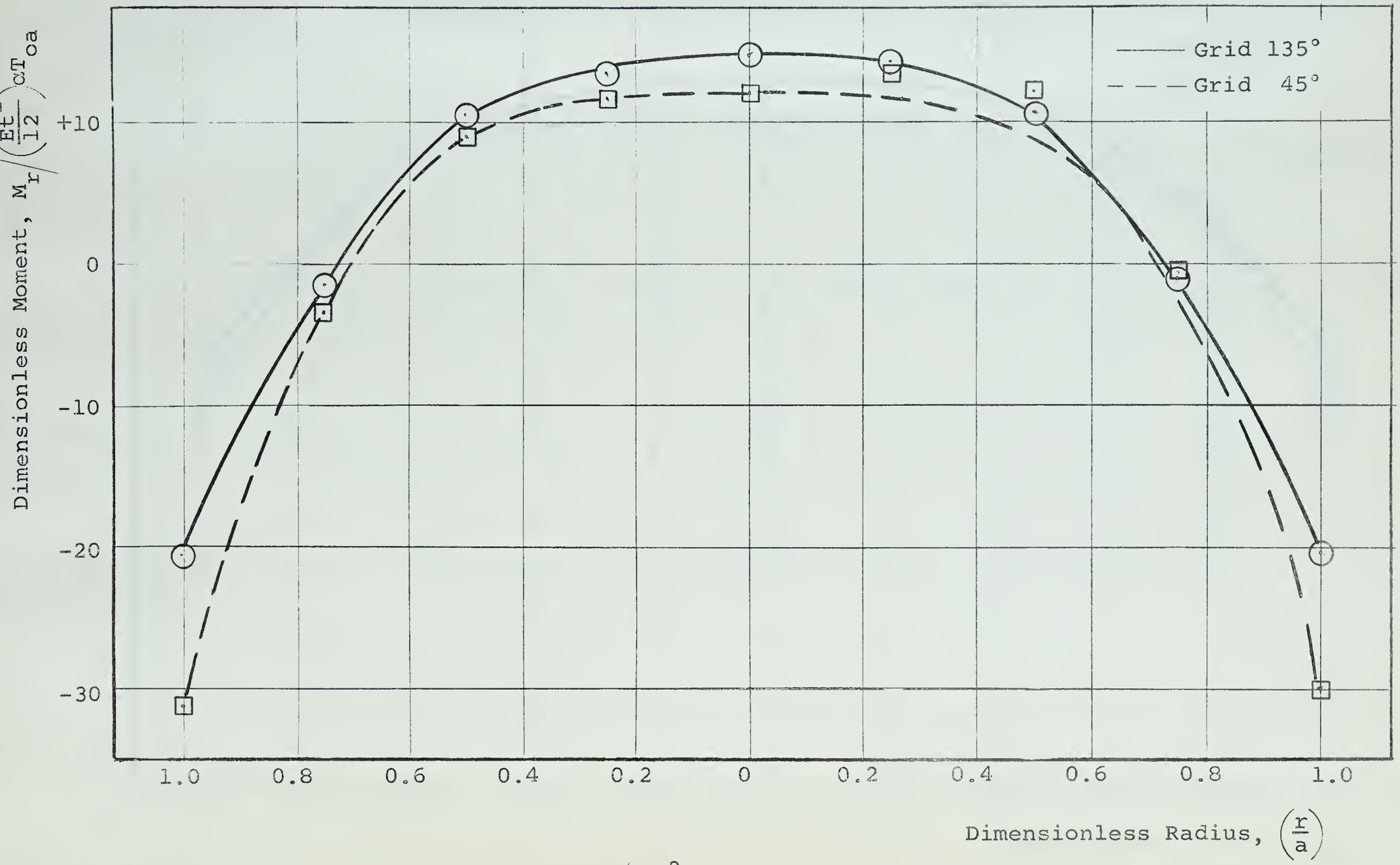

Fig. 36 Dimensionless Moment, $M_r/\left(\frac{Et^2}{12}\right)\alpha T_{oa}$ versus Dimensionless Radius, $\left(\frac{r}{a}\right)$ for the Elastically Supported Circular Plate.

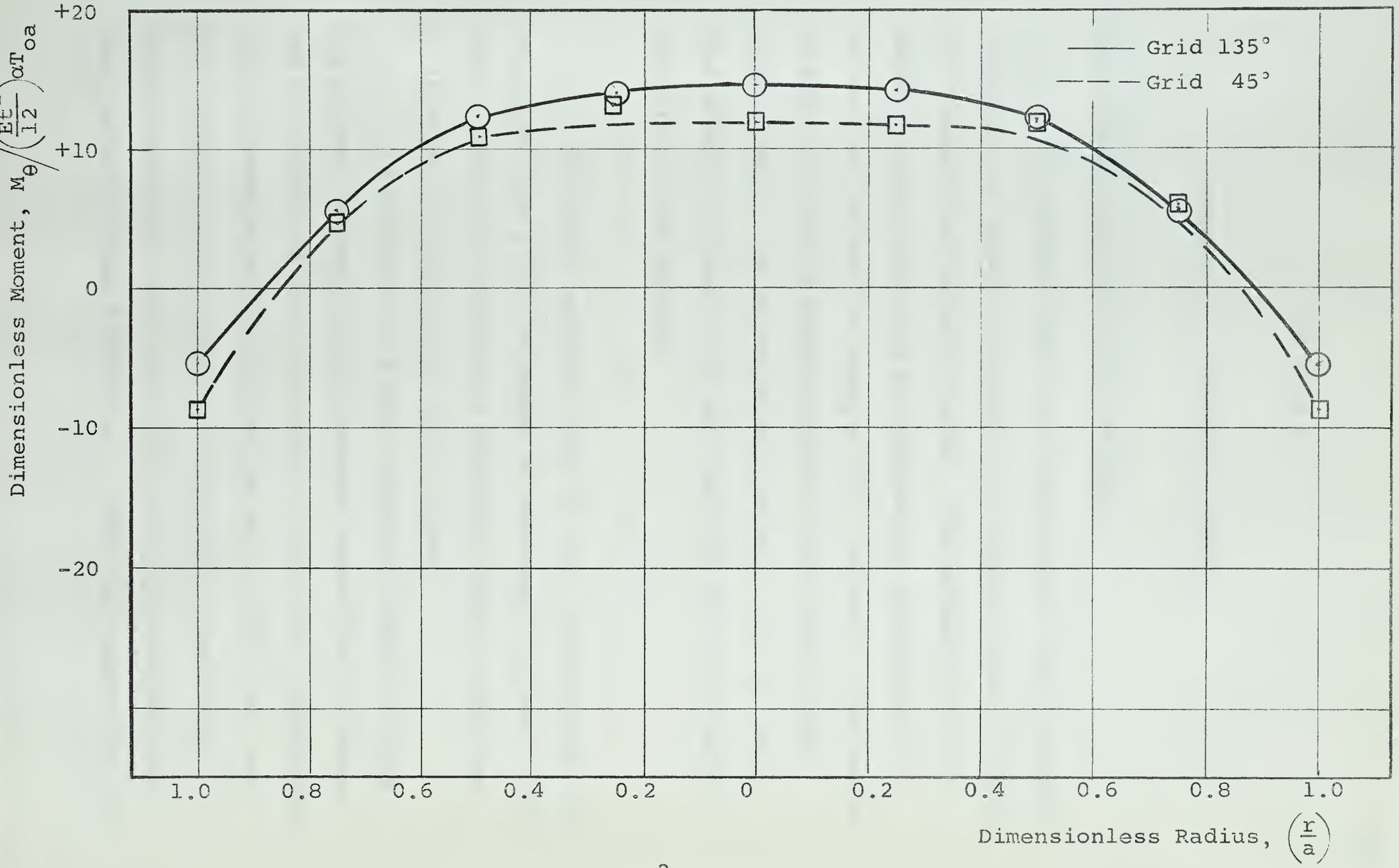

Fig. 37. Dimensionless Moment, $M_\theta \Big/ \left(\frac{Et^2}{12}\right)\alpha T_{oa}$ versus Dimensionless Radius, $\left(\frac{r}{a}\right)$ for the Elastically Supported Circular Plate.

CHAPTER V

SUMMARY AND CONCLUDING REMARKS

5.1 Summary and Concluding Remarks.

1. It appears from this investigation that the Moiré method can be used to determine the deformations of thermally loaded thin metallic plates. The accuracy of the method has been verified by independent measurement of the central deflection using a dial indicator. The number of Moiré fringes is proportional to the slope of the plate, namely, one fringe/0.002 radians. It is noted that several fringes (4-6) are required for the accurate analysis of the results.

2. The model supports used in this investigation did not allow free radial movement at the edge of plate. This radial constraint introduces membrane forces, which tend to increase the deflection of the plate.

In the case of simply supported circular plate, the maximum temperature differences across the thickness and the radius of the plate were 3°F and 32°F, respectively, and the average maximum deflection was 0.02771 in. For the clamped circular plate the respective temperature differences were 1.5°F and 6.25°F, and the avereage maximum deflection was 0.02891 in. The room temperature for

both tests was about 70°F. From this information it is seen that a smaller temperature difference was required for the clamped circular plate in comparison with the simply supported circular plate to produce deflections of the same magnitude. This is largely due to the fact that the clamped circular plate was probably fully constrained from moving radially at the edge, while the simply supported circular plate was only partially constrained from moving radially at the edge.

3. As mentioned in paragraph 2, the ideal boundary conditions were not achieved in this investigation. For this reason the theoretical deflections calculated (pages 74 and 78) bear no relation to the experimental results and this explains the large discrepancy between the two sets of results.

In an attempt to gain an insight into the situation, the following approximate analysis was done.

On the assumption that the boundary did not move and using experimental central deflections it was found that the following two equations closely represent the deflections for the simply supported and clamped circular plates, respectively,

$$w = k_1(r)^{1.5} \quad \text{and} \quad w = k_2(a^2-r^2)^2 ,$$

where k_1 and k_2 are experimental constants.

The lengths of these deflection curves were calculated by

integration. The difference between the lengths of these curves and the original plate diameters is quite small as compared with the diametric thermal expansions calculated for free discs based on the experimental temperature distributions along the middle surface of the plate. This difference can be attributed to two factors: firstly, an increase in the diameter of the model supports due to their increased temperature, and secondly slippage of the plates at the supports. Simple approximate calculations indicate a radial slip of 0.001 in. for the simply supported plate, and a radial slip of 0.0001 in. for the clamped plate.

4. In all the three cases studied the plates were not perfectly flat, and on thermal loading they deflected in the direction of the initial deflection.

5. There is a possibility of some error in the measurement of temperature during the tests. This is probably due to the non-uniformity in the thermocouple junctions, and the poor resolution of the circular scale of the temperature recorder. It was only possible to read within $\pm \frac{1}{4}°F$ on this scale.

6. One of the difficulties in the experimental work was to handle the spot welded thermocouple junctions. These junctions broke very easily, because they were very brittle.

REFERENCES

1. J.E. Goldberg, Axisymmetric Flexural Temperature Stress in Circular Plates", Journal of Applied Mechanics, Vol. 20, pp 257-260. (1953).

2. M. Forray and M. Newmann, "Axisymmetric Bending Stresses in Solid Circular Plates with Thermal Gradients". Journal of Aero Space Sciences, Vol. 27, pp 717-718. (1960).

3. B.A. Boley and J.H. Weiner, "Theory of Thermal Stresses". John Wiley and Sons; New York, 1960.

4. W. Flügge, "Hand-book of Engineering Mechanics". McGraw Hill Book Co; New York, 1962.

5. G. Gerard and A.C. Gilbert, "Photothermoelasticity: An Exploratory Study". Journal of Applied Mechanics, Vol. 24, pp 355-360 (1957).

6. H. Becker and A.C. Colao, "Photothermoelastic Investigation of Thermal Stresses in Flat Plates". Journal of Basic Engineering, Vol. 85, pp 566-568. (1963).

7. P.K. Ligtenberg, "The Moiré Method - new experimental Method for determination of moments in small slab models". Proceedings of the Society for Experimental Stress Analysis, Vol. 12, No. 2, pp 83-98. (1954).

8. W.A. Bradley, "Laterally Loaded Thin Flat Plates". Proceedings of A.S.C.E. (EM) Vol. 85, pp 77-107. (1959).

9. H.Y. Tso, "A Study of Laterally Loaded Thin Flat Plates by the Moiré Method". Master's Thesis, University of Alberta, 1963.

10. O.C. Zienkiewicz and C. Cruz, "The Use of the Slab Analogy in the determination of Thermal Stresses". International Journal of Mechanical Sciences, Vol. 4, pp 285-296. (1962)

11. C.A.Sciammarella and B.E. Ross, "Thermal Stresses in Cylinders by the Moiré Method". Proceedings of the Society for Experimental Stress Analysis, Vol. 21, No. 2, pp 289-296. (1964).

12. J.N. Goodier, "Thermal Stress and Deformation". Journal of Applied Mechanics, Vol. 23, pp 467-474. (1957).

13. W.A. Bradley, "The determination of moments and deflections in plates by the Moire method and by Finite Difference with application to the square clamped plate with square cutouts". Doctoral Thesis, University of Michigan, 1956.

14. S. Timoshenko, "Theory of Plates and Shells". McGraw Hill Book Co., New York, 1959.

APPENDIX

(Data and Numerical Results)

TABLE A.1 TEMPERATURE DISTRIBUTION FOR THE SIMPLY SUPPORTED CIRCULAR PLATE.

Radial Distance (Inch)	Temperature On hot side (°F)	Average Temperature On hot side (°F)	Temperature On cold side (°F)	Average Temperature On Cold side (°F)	Average ΔT (°F)
4.539	123	122.5	123	122.5	0
4.0	125	124.5	124.5	124	0.5
3.0	134.5	133.25	133.5	133.25	1.0
2.0	144.5	143.5	142.5	141.75	1.75
1.0	150	151.5	148.5	149.5	2.0
0	156	156	153	153	3.0
1.0	153		150.5		
2.0	142.5		141		
3.0	132		131		
4.0	124		123.5		
4.539	122		122		

Initial plate temperature = 70°F.

Final plate temperature = 71°F.

Table A.2 DIMENSIONLESS DEFLECTIONS AND BENDING MOMENTS FOR THE SIMPLY SUPPORTED CIRCULAR PLATE.

Radius (Inch)	Dimensionless Deflection, $\frac{Wt}{a^2 \alpha T_{D(o)}}$		Dimensionless Moment, $\frac{M_r}{\left(\frac{Et^2}{12}\right)\alpha T_{D(o)}}$		Dimensionless Moment, $\frac{M_\theta}{\left(\frac{Et^2}{12}\right)\alpha T_{D(o)}}$	
	Grid Vertical	Grid Horizontal	Grid Vertical	Grid Horizontal	Grid Vertical	Grid Horizontal
4.539	0	0	1.0462	1.0462	3.1691	3.1691
4.0	0.3297	0.3297	1.1138	1.1138	3.3967	3.3967
3.0	0.940	0.936	1.6518	1.4942	4.3649	4.3725
2.0	1.524	1.522	3.9615	3.6915	6.3951	6.5454
1.0	1.975	1.983	7.7028	7.8582	8.9547	9.3268
0	2.142	2.167	9.9833	10.8443	9.9833	10.8443
1.0	1.975	1.983	8.699	7.6442	8.8684	8.6797
2.0	1.524	1.522	3.8355	3.9845	6.4005	6.4670
3.0	0.940	0.936	1.6141	1.4942	4.3487	4.2765
4.0	0.3297	0.3297	1.1138	1.1138	3.3967	3.3967
4.539	0	0	1.0462	1.0462	3.1691	3.1691

Table A.3 COMPARISON OF DEFLECTIONS BY MOIRÉ METHOD AND THEORY* FOR THE SIMPLY SUPPORTED CIRCULAR PLATE.

Radius (Inch)	Moiré Deflection, w (Inch)		Average Moiré Deflection, w (Inch)		Theoretical Deflection, w (Inch)
	Grid Vertical	Grid Horizontal	Grid Vertical	Grid Horizontal	
4.539	0	0	0	0	0
4.0	0.00428	0.00428	0.00424	0.00424	0.000527
3.0	0.01216	0.01208	0.01209	0.01204	0.001437
2.0	0.01972	0.01970	0.01960	0.01957	0.002205
1.0	0.02556	0.02574	0.02540	0.02550	0.002695
0	0.02755	0.02787	0.02755	0.02787	0.002864
1.0	0.02524	0.02526			0.002695
2.0	0.01948	0.01944			0.002205
3.0	0.01202	0.01200			0.001437
4.0	0.00420	0.00420			0.000527
4.539	0	0			0

* Based on equation (3).

Table A.4 COMPARISON OF DIMENSIONLESS BENDING MOMENTS BY MOIRÉ METHOD AND THEORY* FOR THE SIMPLY SUPPORTED CIRCULAR PLATE.

Radius (Inch)	Dimensionless Moment, $M_r \Big/ \left(\frac{Et^2}{12}\right)\alpha T_{D(o)}$ By Moiré Method		Dimensionless Moment, $M_r \Big/ \left(\frac{Et^2}{12}\right)\alpha T_{D(o)}$ By Theory	Dimensionless Moment, $M_\theta \Big/ \left(\frac{Et^2}{12}\right)\alpha T_{D(o)}$ By Moiré Method		Dimensionless Moment, $M_\theta \Big/ \left(\frac{Et^2}{12}\right)\alpha T_{D(o)}$ By Theory
	Grid Vertical	Grid Horizontal		Grid Vertical	Grid Horizontal	
4.539	1.0462	1.0462	0	3.1691	3.1691	+0.3340
4.0	1.1138	1.1138	-0.0389	3.3967	3.3967	+0.2062
3.0	1.6518	1.4942	-0.0943	4.3649	4.3725	+0.0950
2.0	3.9615	3.6915	-0.1428	6.3951	6.5454	-0.1066
1.0	7.7028	7.8582	-0.1354	8.9547	9.3268	-0.1973
0	9.9833	10.8443	-0.3330	9.9833	10.8443	-0.3330
1.0	8.699	7.6442	-0.1354	8.8684	8.6797	-0.1973
2.0	3.8355	3.9845	-0.1428	6.4005	6.4670	-0.1066
3.0	1.6141	1.4942	-0.0943	4.3487	4.2765	+0.0950
4.0	1.1138	1.1138	-0.0389	3.3967	3.3967	+0.2062
4.539	1.0462	1.0462	0	3.1691	3.1691	+0.3340

* Based on equations (5).

Table A.5 TEMPERATURE DISTRIBUTION FOR THE CLAMPED CIRCULAR PLATE.

Radial Distance (Inch)	Temperature On hot side (°F)	Average Temperature On hot side (°F)	Temperature on cold side (°F)	Average Temperature on cold side (°F)	Average ΔT (°F)
4.5	91.5	91.5	90.5	90.5	1.0
4.0	92	92	90.5	90.75	1.25
3.0	93.5	93.25	93	92.75	0.5
2.0	95	95.25	94	94.25	1.0
1.0	97.5	97	96	96	1.0
0	98	98	96.5	96.5	1.5
1.0	96.5		96		
2.0	95.5		94.5		
3.0	93		92.5		
4.0	92		91.0		
4.5	91.5		90.5		

Initial plate temperature = 68°F.

Final plate temperature = 70°F.

Table A.6 DIMENSIONLESS DEFLECTIONS AND BENDING MOMENTS FOR THE CLAMPED CIRCULAR PLATE.

Radius (Inch)	Dimensionless Deflection, $w/a^2\alpha T_{D(o)}$		Dimensionless Moment, $M_r/\left(\frac{Et^2}{12}\right)\alpha T_{D(o)}$		Dimensionless Moment, $M_\theta/\left(\frac{Et^2}{12}\right)\alpha T_{D(o)}$	
	Grid Vertical	Grid Horizontal	Grid Vertical	Grid Horizontal	Grid Vertical	Grid Horizontal
4.5	0	0	-69.243	-41.406	-23.512	-14.330
4.0	0.2405	0.1471	-25.576	-18.666	-4.386	-4.142
3.0	1.587	1.028	-1.986	-8.589	+9.360	+5.267
2.0	3.132	2.462	+13.820	+13.317	+19.048	+19.072
1.0	4.276	3.778	+21.309	+20.543	+22.125	+27.384
0	4.718	4.430	+22.893	+53.974	+22.893	+53.974
1.0	4.276	3.778	+22.499	+21.978	+24.185	+29.009
2.0	3.132	2.462	+14.036	+12.318	+18.926	+19.353
3.0	1.587	1.028	-1.677	-10.426	+9.526	+4.174
4.0	0.2405	0.1471	-24.631	-18.458	-4.156	-4.472
4.5	0	0	-68.811	-41.190	-23.372	-14.258

Table A.7 COMPARISON OF DEFLECTIONS BY MOIRÉ METHOD AND THEORY* FOR THE CLAMPED CIRCULAR PLATE.

Radius (Inch)	Moiré Deflection, w (Inch)		Average Moiré Deflection, w (Inch)		Theoretical Deflection, w, (Inch)
	Grid Vertical	Grid Horizontal	Grid Vertical	Grid Horizontal	
4.5	0	0	0	0	0
4.0	0.00148	0.00100	0.00152	0.00093	0.0009×10^{-4}
3.0	0.01002	0.00684	0.01003	0.00650	0.353×10^{-4}
2.0	0.01952	0.01602	0.01980	0.01556	0.854×10^{-4}
1.0	0.02682	0.02412	0.02703	0.02388	1.242×10^{-4}
0	0.02982	0.02800	0.02982	0.02800	1.569×10^{-4}
1.0	0.02724	0.02364			1.242×10^{-4}
2.0	0.02008	0.01510			0.854×10^{-4}
3.0	0.01004	0.00616			0.353×10^{-4}
4.0	0.00156	0.00086			0.0009×10^{-4}
4.5	0	0			0

* Based on equation (3).

Table A.8 COMPARISON OF DIMENSIONLESS BENDING MOMENTS BY MOIRÉ METHOD AND THEORY* FOR THE CLAMPED CIRCULAR PLATE.

Radius (Inch)	Dimensionless Moment, $M_r / \left(\frac{Et^2}{12}\right)\alpha T_{D(o)}$ By Moiré Method		Dimensionless Moment, $M_r / \left(\frac{Et^2}{12}\right)\alpha T_{D(o)}$ By Theory	Dimensionless Moment, $M_\theta / \left(\frac{Et^2}{12}\right)\alpha T_{D(o)}$ By Moiré Method		Dimensionless Moment, $M_\theta / \left(\frac{Et^2}{12}\right)\alpha T_{D(o)}$ By Theory
	Grid Vertical	Grid Horizontal		Grid Vertical	Grid Horizontal	
4.5	-69.243	-41.406	-1.0092	-23.512	-14.330	-0.9997
4.0	-25.576	-18.666	-1.0189	-4.886	-4.142	-0.9900
3.0	-1.986	-8.589	-1.0389	+9.360	+5.267	-0.9700
2.0	+13.820	+13.317	-1.0597	+19.048	+19.072	-0.9659
1.0	+21.309	+20.543	-1.1121	+22.125	+27.384	-1.1051
0	+22.893	+53.974	-1.1711	+22.893	+53.974	-1.1711
1.0	+22.499	+21.978	-1.1121	+24.185	+29.009	-1.1051
2.0	+14.036	+12.318	-1.0597	+18.926	+19.353	-0.9659
3.0	-1.677	-10.426	-1.0389	+9.526	+4 174	-0.9700
4.0	-24.631	-18.458	-1.0189	-4.156	-4.472	-0.9900
4.539	-68.811	-41.190	-1.0092	-23.372	-14.258	-0.9997

* Based on equations (5).

Table A.9 TEMPERATURE DISTRIBUTION FOR THE ELASTICALLY SUPPORTED CIRCULAR PLATE.

Radius (Inch)	Temperature for 0° and 90° Grid Directions (°F)	Average Temperature for 0° and 90° Grid Directions (°F)	Temperature for 45° and 135° Grid Directions (°F)	Average Temperature for 45° and 135° Grid Directions (°F)
4.008	106	106.25	97	97
3.0	105.5	105.5	96.5	96.25
2.0	104.5	104.25	96	95.75
1.0	103.5	103.25	94.5	94.35
0	103	103	94	94
1.0	103		94.2	
2.0	104		95.5	
3.0	105.5		96	
4.008	106.5		97	

For 0° and 90° grid directions test,

Initial plate temperature = 70°F.
Final plate temperature = 72°F.

For 45° and 135° grid directions test,

Initial plate temperature = 67°F.
Final plate temperature = 66°F.

Table A.10 DIMENSIONLESS DEFLECTIONS AND BENDING MOMENTS FOR THE ELASTICALLY SUPPORTED CIRCULAR PLATE, FOR HORIZONTAL AND VERTICAL GRID DIRECTIONS.

Radius (Inch)	Dimensionless Deflection, $\frac{Wt}{a^2 \alpha T_{oa}}$		Dimensionless Moment, $\frac{M_r}{\left(\frac{Et^2}{12}\right)\alpha T_{oa}}$		Dimensionless Moment, $\frac{M_\theta}{\left(\frac{Et^2}{12}\right)\alpha T_{oa}}$	
	Grid Vertical	Grid Horizontal	Grid Vertical	Grid Horizontal	Grid Vertical	Grid Horizontal
4.008	0	0	-64.167	-25.273	-19.699	-6.865
3.0	0.8954	0.8811	-2.038	-2.049	+5.834	+5.977
2.0	2.1265	2.0661	+7.331	+10.930	+12.355	+12.508
1.0	3.1266	2.8992	+16.206	+14.036	+16.852	+14.036
0	3.4757	3.2172	+16.684	+13.947	+16.684	+13.947
1.0	3.1302	2.9489	+16.140	+13.97	+16.830	+13.925
2.0	2.1655	2.1016	+7.264	+10.800	+12.334	+13.012
3.0	0.9273	0.8882	-1.739	-1.921	+6.109	+6.093
4.008	0	0	-62.923	-25.074	-19.289	-6.77

Table A.11 DIMENSIONLESS DEFLECTIONS AND BENDING MOMENTS FOR THE ELASTICALLY SUPPORTED CIRCULAR PLATE, FOR 45° and 135° GRID DIRECTIONS.

Radius (Inch)	Dimensionless Deflection, $Wt / a^2 \alpha T_{oa}$		Dimensionless Moment, $M_r / \left(\frac{Et^2}{12}\right) \alpha T_{oa}$		Dimensionless Moment, $M_\theta / \left(\frac{Et^2}{12}\right) \alpha T_{oa}$	
	Grid at 45°	Grid at 135°	Grid at 45°	Grid at 135°	Grid at 45°	Grid at 135°
4.008	0	0	-31.334	-20.692	-8.742	-5.229
3.0	0.8199	0.8795	-3.478	-1.672	+4.80	+5.711
2.0	1.9014	2.0150	+8.814	+10.417	+10.886	+12.247
1.0	2.6674	2.8098	+11.481	+13.268	+13.047	+13.414
0	2.9272	3.0889	+11.810	+14.535	+11.810	+14.535
1.0	2.6790	2.7887	+13.275	+14.021	+11.589	+14.239
2.0	1.9688	1.9476	+11.949	+10.345	+12.031	+12.321
3.0	0.8468	0.8064	-1.6718	-1.479	+5.711	+5.616
4.008	0	0	-31.154	-20.656	-8.682	-5.218